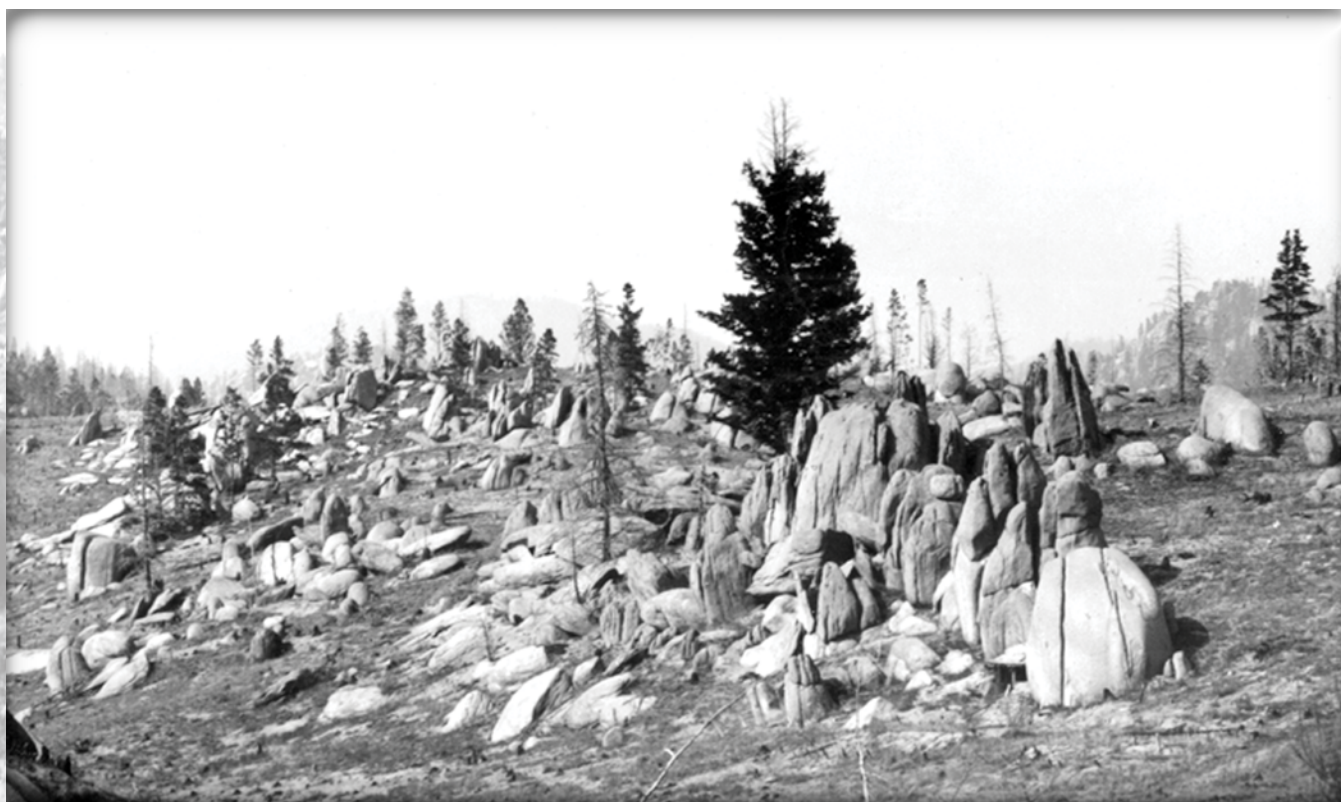# Control of Precambrian Basement Deformation Zones on Emplacement of the Laramide Boulder Batholith and Butte Mining District, Montana, United States

Scientific Investigations Report 2011–5016

Control of Precambrian Basement Deformation Zones on Emplacement of the Laramide Boulder Batholith and Butte Mining District, Montana, United States

By Byron R. Berger, Thomas G. Hildenbrand, and J. Michael O'Neill

U.S. Department of the Interior
KEN SALAZAR, Secretary

U.S. Geological Survey
Marcia K. McNutt, Director

U.S. Geological Survey, Reston, Virginia: 2011

Contents

Figures

Abbreviations Used in This Report

2D	two-dimensional
3D	three-dimensional
A	Avon, Montana
A/m	ampere-turn per meter
Ag	silver
AN	Anaconda mine
AR	Archean rocks
As	arsenic
BB	Boulder batholith
BH	Big Hole Valley
BP	Burton Park pluton
CG	Climax Gulch pluton
Cu	copper
D	Donald pluton
DL	Deer Lodge Valley
FS	Fleecer Stock
Ga	giga-annum
GC	Clark Fork River valley
GFTZ	Great Falls tectonic zone
GL	Garnet line
HC	Hell Canyon pluton
HM	Highland Mountains
IB	Idaho batholith
IGSN	International Gravity Standardization Net
K	Kelley mine
kg/m³	kilogram per cubic meter
km	kilometer
KR	Kokoruda Ranch Complex
kt	kiloton
L2	Leonard No. 2 mine
LT	Lombard thrust
LX	Lexington mine
M	magnetic susceptibility
m	meter
m.y.	million year (duration)
Ma	mega-annum (point in time)

MC	Moose Creek pluton
mG	milligal
MN	Mountain Consolidated mine
Moz	megaounce
Mt	megaton
nT	nanotesla
P	Proterozoic Belt Basin rocks
Pb	lead
PB	Pioneer batholith
PL	Perry line
RC	Rader Creek Granodiorite pluton
S	Steward mine
Sr	strontium
SWMTZ	southwest Montana tectonic zone
SWS	Silver Wave stock
TR, TB	Tobacco Root batholith
TRM	Tobacco Root Mountains
U	Unionville Granodiorite pluton
U	uranium
Zn	zinc
ρ	density

Control of Precambrian Basement Deformation Zones on Emplacement of the Laramide Boulder Batholith and Butte Mining District, Montana, United States

By Byron R. Berger, Thomas G. Hildenbrand, and J. Michael O'Neill

Abstract

What are the roles of deep Precambrian basement deformation zones in the localization of subsequent shallow-crustal deformation zones and magmas? The Paleoproterozoic Great Falls tectonic zone and its included Boulder batholith (Montana, United States) provide an opportunity to examine the importance of inherited deformation fabrics in batholith emplacement and the localization of magmatic-hydrothermal mineral deposits. Northeast-trending deformation fabrics predominate in the Great Falls tectonic zone, which formed during the suturing of Paleoproterozoic and Archean cratonic masses approximately 1,800 mega-annum (Ma). Subsequent Mesoproterozoic to Neoproterozoic deformation fabrics trend northwest. Following Paleozoic through Early Cretaceous sedimentation, a Late Cretaceous fold-and-thrust belt with associated strike-slip faulting developed across the region, wherein some Proterozoic faults localized thrust faulting, while others were reactivated as strike-slip faults. The 81- to 76-Ma Boulder batholith was emplaced along the reactivated central Paleoproterozoic suture in the Great Falls tectonic zone. Early-stage Boulder batholith plutons were emplaced concurrent with east-directed thrust faulting and localized primarily by northwest-trending strike-slip and related faults. The late-stage Butte Quartz Monzonite pluton was localized in a northeast-trending pull-apart structure that formed behind the active thrust front and is axially symmetric across the underlying northeast-striking Paleoproterozoic fault zone, interpreted as a crustal suture. The modeling of potential-field geophysical data indicates that pull-apart–stage magmas fed into the structure through two funnel-shaped zones beneath the batholith. Renewed magmatic activity in the southern feeder from 66 to 64 Ma led to the formation of two small porphyry-style copper-molybdenum deposits and ensuing world-class polymetallic copper- and silver-bearing veins in the Butte mining district. Vein orientations parallel joints in the Butte Quartz Monzonite that, in turn, mimic Precambrian deformation fabrics found outside the district. The faults controlling the Butte veins are interpreted to have formed through activation under shear of preexisting northeast-striking joints as master faults from which splay faults formed along generally east-west and northwest joint plane orientations.

Introduction

The reactivation of Precambrian deep-crustal deformation zones, often bounding tectonic terranes, has long been hypothesized to play a role in subsequent shallow-crustal faulting, the emplacement of plutons, and the structural localization of magmatic-hydrothermal mineral deposits (for example, Billingsley and Locke, 1941). Although multiple studies have demonstrated a spatial correlation between basement deformation zones and mining districts (for example, Grauch and others, 2003; O'Neill and others, 2004; Emsbo and others, 2006), few studies relate basement deformation fabrics to the structural control on mineralized plutonic rock complexes. In this report we use potential-field geophysical data to interpret the structural control on plutons, dikes, and mineral deposits in the Late Cretaceous Boulder batholith, Montana, in the context of Precambrian basement deformation zones. We also interpret the structural controls on postbatholith Paleocene dike emplacement and mineralized veins in the batholith-hosted Butte mining district.

The discussion covers the following: (1) the predominant deformation fabrics and their evolution in Proterozoic basement rocks in southwest Montana; (2) the evidence for the reactivation of many Precambrian structures during Late Cretaceous deformation in southwest Montana; (3) a proposed two-stage model for the structural controls on the emplacement of the Boulder batholith; and (4) a new model for the structural evolution of the vein systems in the Butte mining district.

Paleoproterozoic Tectonics in Southwestern Montana

The collision of an Archean terrane and a Paleoprotero-zoic terrane about 1,800 mega-annum (Ma) created a north-east-trending deformation zone 1,500 kilometers (km) long by as much as 200 km wide known as the Great Falls tectonic zone (O'Neill and Lopez, 1985) (fig. 1). An abrupt change across this belt in the antiquity of upper intercept dates of uranium-lead (U-Pb) zircon ages (fig. 2) and a belt of volcanic and plutonic rocks led O'Neill (1998) to postulate that the principal fault boundary or suture underlies the central axis of the tectonic zone.

Ductile and brittle deformation, igneous intrusive activity, and metamorphism characterize the Great Falls tectonic zone deformation (O'Neill, 1998). Collision-related deformation fabrics are well exposed in mountain ranges at the southern end of the Late Cretaceous Boulder batholith (fig. 2), in what is known as the Highland Mountains, and farther southeast in the Tobacco Root Mountains that host the Tobacco Root batholith (fig. 2). In the Highland Mountains the deforma-tion is complex, but, overall, foliation strikes northeast to east-northeast. Paleoproterozoic mafic dikes and sills intruded subparallel to the foliation. To the east and southeast in the Tobacco Root Mountains, directly east of the Highland Mountains, foliation and dikes trend east-northeast and west-northwest and, farther south, trend northeast. From such map data, we infer that the regionally predominant, underlying Paleoproterozoic fabric in the Archean rocks trends northeast parallel to the main tectonic suture, except in the Highland and northern Tobacco Root Mountains, where a generally east-west fabric dominates. Figure 3 illustrates the character of this likely regional pattern in an area at the south end of the Tobacco Root Mountains.

Mesoproterozoic Tectonics in Southwestern Montana

A northwest-trending depositional trough, referred to as the Belt Basin (for example, Harrison, 1972), began to form across the Great Falls tectonic zone at approximately 1,500 Ma (fig. 4). The northeast edge of the basin trends northwest, parallel to the basin axis, and may have a structural root. Northwest-striking faults with Proterozoic ancestry—the Lewis and Clark line—are exposed in the west-central (see Harrison, 1972) and southeast parts of the basin (see Schmidt and Garihan, 1986). Mesoproterozoic and Neoproterozoic diabase dikes are within or parallel to the faults (Schmidt and Garihan, 1986). Figure 5 shows the orientations of dikes in the Highland Mountains and nearby Tobacco Root Mountains. In the southeast part of the basin in what is called the Helena

embayment, systematic changes in the thicknesses of basin sediments are suggestive of the importance of east-west faults with normal-sense displacement (Winston, 1986). The spatial correlation of east-west Mesoproterozoic faulting with Paleo-proterozoic east-west foliation in the Highland and northern Tobacco Root Mountains is suggestive of a Paleoproterozoic ancestry to the Helena embayment.

Late Cretaceous Tectonics in Southwestern Montana

Beginning in the Late Cretaceous and continuing into the early Eocene, a period known as the Laramide, there was significant tectonic and magmatic activity in western Mon-tana (fig. 6). East- to northeast-directed thrust faults that are younger to the east accommodated east-west compression. The thrust front north of the Boulder batholith, labeled the Mon-tana disturbed belt on figure 6, corresponds to the northeast edge of the Proterozoic Belt Basin. The coincidence of the basin edge and frontal thrusts is suggestive that a northwest-trending tectonic inheritance guided the frontal thrust zone immediately east of the Boulder batholith.

East of the Boulder batholith, the north and south normal-fault boundaries of the Helena embayment (fig. 4) were reactivated as strike-slip and reverse-slip fault zones to form the Helena structural salient of the frontal thrust zone (fig. 6). These transverse zones consist of anastomosing systems of faults (see Schmidt and O'Neill, 1982). Within the salient, northwest-striking strike-slip faults accommodated shortening strains west of the thrust front.

On the foreland southeast of the Boulder batholith and south of the Willow Creek fault zone, the principal mechanism of shortening east of the thrust front was northwest-striking left-reverse (oblique) faults (fig. 5). Schmidt and Garihan (1986) documented a significant difference in the offset of Archean marker units relative to overlying Paleozoic units, indicating the northwest faults are Meso- to Neoproterozoic faults that have been reactivated.

Initially, thrust faulting with very local strike-slip dis-placements was the primary mechanism for accommodating Late Cretaceous regional strains. As the thrust front advanced farther east, strain accommodation behind it was predomi-nantly on northwest-striking strike-slip faults. North and northwest of the Boulder batholith, where Cretaceous plutonic rocks are scarce, there is an approximately 440-km-long zone of strike-slip and related faulting known as the Lewis and Clark line (fig. 6). The Neoproterozoic age and intermittent Phanerozoic reactivation of some faults in the Lewis and Clark line were documented by Hobbs and others (1965) near its western end, and Reynolds (1979) documented activity of a similar age at the eastern end.
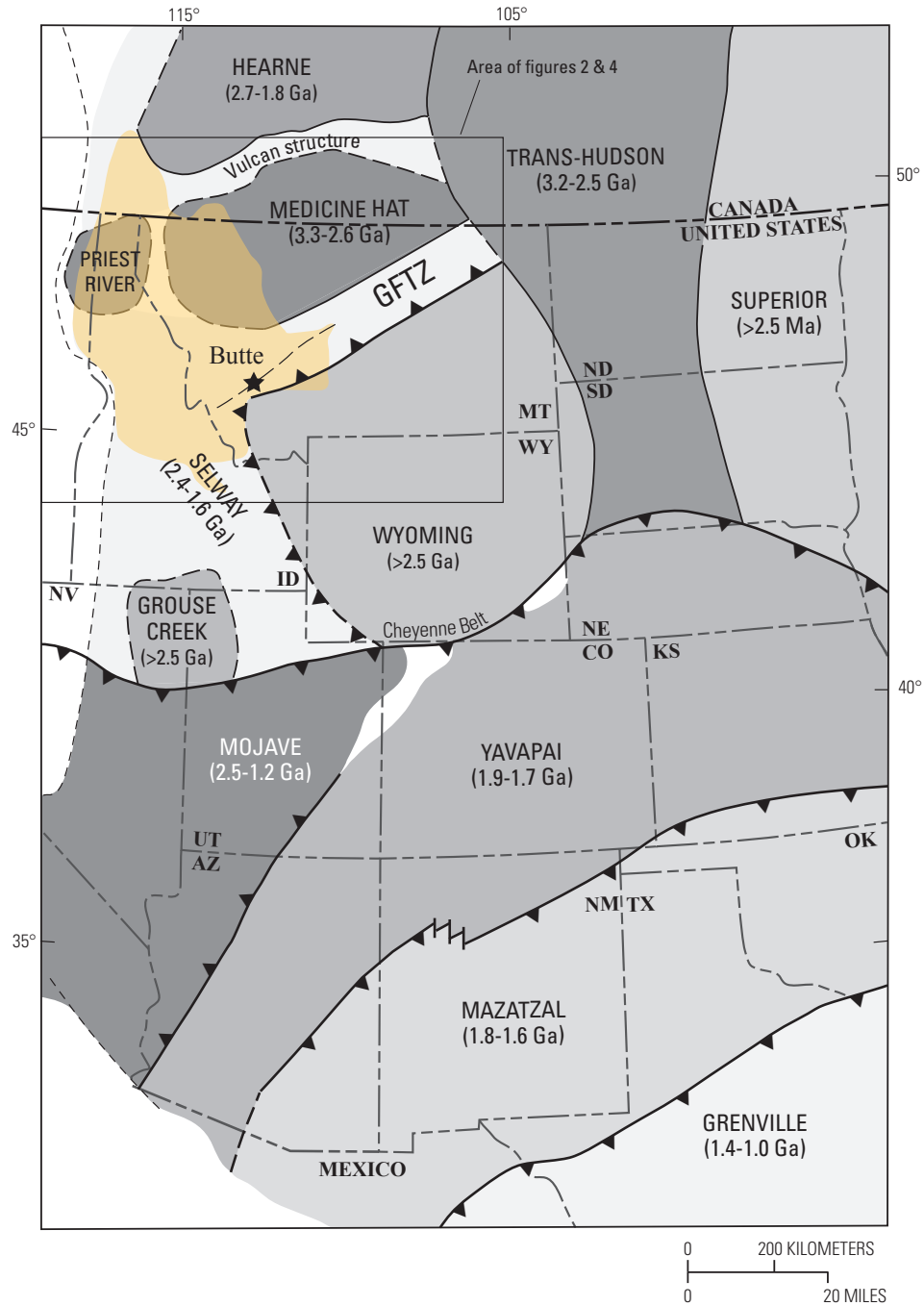
Figure 1. Precambrian basement terranes of the western United States showing the location of the Great Falls tectonic zone (GFTZ), the Butte mining district (star symbol), and the Proterozoic Belt Basin. (Ga, giga-annum; Ma, mega-annum; Sr, strontium; after Karlstrom and Humphreys, 1998; Eisele and Isachsen, 2001; Foster and others, 2006).
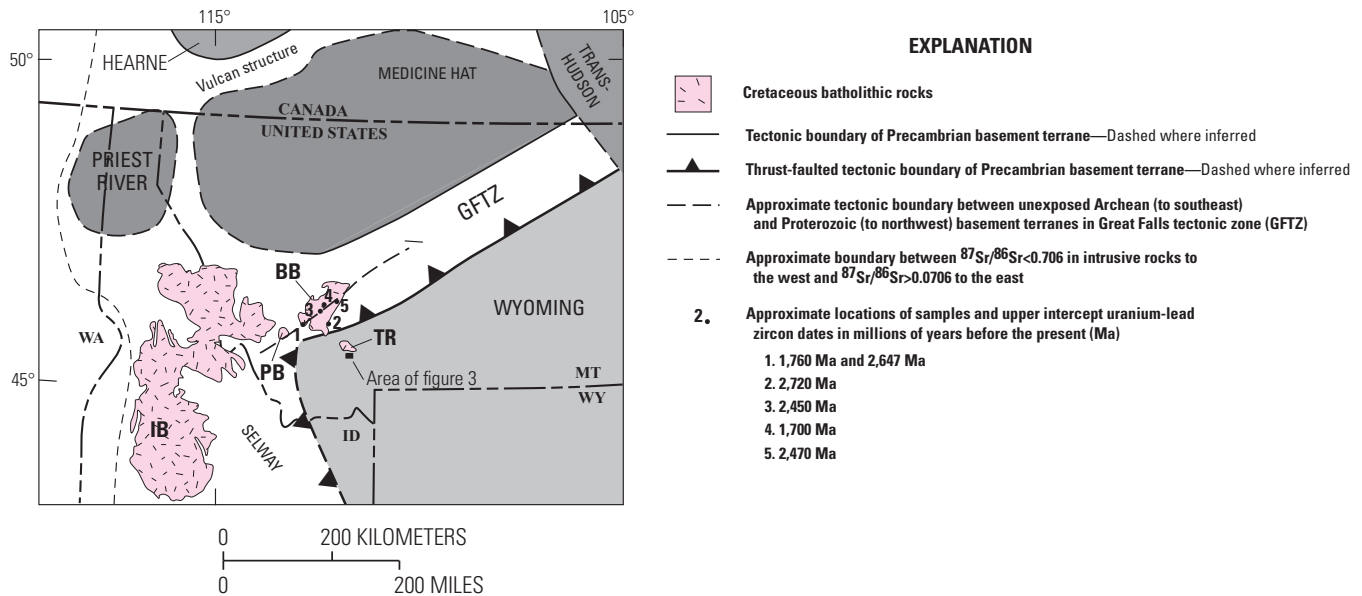
Figure 2. Upper intercept zircon dates from intrusive rocks in the Great Falls tectonic zone (GFTZ). The terranes and boundaries are as shown for the figure 2 reference area in figure 1 (BB, Boulder batholith; IB, Idaho batholith; PB, Pioneer batholith; TR, Tobacco Root batholith; data from Lund and others, 2002; Murphy and others, 2002).

The Boulder Batholith

Plutonism and cogenetic volcanism in the Boulder batholith began approximately 81 Ma (Tysdal, 1998) and continued until approximately 74 Ma (Lund and others, 2002). The batholith (fig. 7), elongated northeast-southwest, is approximately 90 km long and 50 km wide. Based on differing styles of structural control on pluton emplacement, the plutonic rocks are subdivided into two groups, an early stage and a younger Butte Quartz Monzonite stage. Early-stage plutons span the approximate interval of 81–76 Ma (Lund and others, 2002), while the more voluminous Butte Quartz Monzonite was emplaced over a shorter interval at approximately 75–74 Ma (Lund and others, 2002).

Tectonic and Structural Localization of Early-Stage Magmas

Initially, early-stage magmas were emplaced concurrently with superjacent thrust faulting and related folding. The oldest cogenetic Elkhorn Mountains Volcanics are folded and uncon-formably overlain by younger Elkhorn Mountains Volcanics that are not folded (Smedes, 1966). Thrust faults occurring after sill emplacement commonly juxtapose Elkhorn Mountains Volcanics and sills. Many sills can be traced back into plutons with lineation fabrics (Smedes, 1966). The thrust faults propagated folds in the upper and lower plates, and Klepper and others (1957) documented north-trending synvolcanic fold

axes and concurrent reverse faulting, indicating that folding, faulting, and intrusion were synchronous in many instances. This finding is consistent with observed thrust-faulted, sill/host-rock contacts that postdate sill emplacement (Smedes, 1966). Paleomagnetic studies show that some sills were folded after emplacement while others intruded into folded rocks (S. Harlan, George Mason University, personal commun., 2005).

Many early-stage plutons cut and offset thrust faults and related sill complexes and were clearly emplaced after local thrust faulting (fig. 8). Many of these plutons and related hydrothermal veins strike northwest parallel to high-angle faults. At some localities, screens of Elkhorn Mountains Volcanics have a strong northwest-trending shear fabric, and adjacent northwest-southeast–elongated intrusions have a distinct contact-zone foliation, both abruptly terminated at a sharp, northeast-striking contact with the younger stage Butte Quartz Monzonite. These data are suggestive that the plutons were localized by northwest-striking faults.

The localization of early-stage intrusions by post-thrust faulting, northwest-striking faults characterizes much of the east and south margins of the Boulder batholith (see Klepper and others, 1957; Prostka, 1966; Smedes, 1966; Tilling, 1968; Klepper and others, 1971b). Figure 8 shows the relation of early-stage intrusions and associated hydrothermal veins to northwest-striking faults along the east margin of the batho-lith. The Silver Wave stock (SWS in fig. 8) is localized along the left-lateral Indian Creek fault zone. The Indian Creek zone offsets reverse faults and early-stage sills. At the south end of the batholith, the Donald and Hell Canyon plutons (fig. 7) are

EXPLANATION

Cenozoic | Cenozoic volcanic and surficial deposits, undifferentiated

Proterozoic | Pegmatite dike, Mesoproterozoic(?)

Archean | Quartzofeldspathic gneiss, undifferentiated

Amphibolite—Dotted where in subcrop

Dolomitic marble—Dotted where in subcrop

Ultramafic rocks, undifferentiated

45 — Strike and dip of foliation

20 — Lineation showing plunge

— Zone of shear

— Fault

— Orogenic quartz vein, auriferous, dotted where in subcrop

112°00'

45°17'30"

0   0.5   1 KILOMETER

0   0.5   1 MILE

Figure 3. Lineations, foliations, and orogenic gold veins in Archean rocks in the southernmost Tobacco Root Mountains (from Weir, 1982). The location of this figure is shown on figure 2, and the location of the Tobacco Root Mountains is shown by the symbol TRM on figure 5. Syntectonic, reverse-fault–controlled auriferous quartz-sulfide-carbonate-fuchsite veins are indicated by red lines. The abundant west-northwest–east-southeast trending pegmatite dikes are 1,572±51 Ma (mega-annum) (Cole, 1983) and represent an imposed Mesoproterozoic structural fabric.
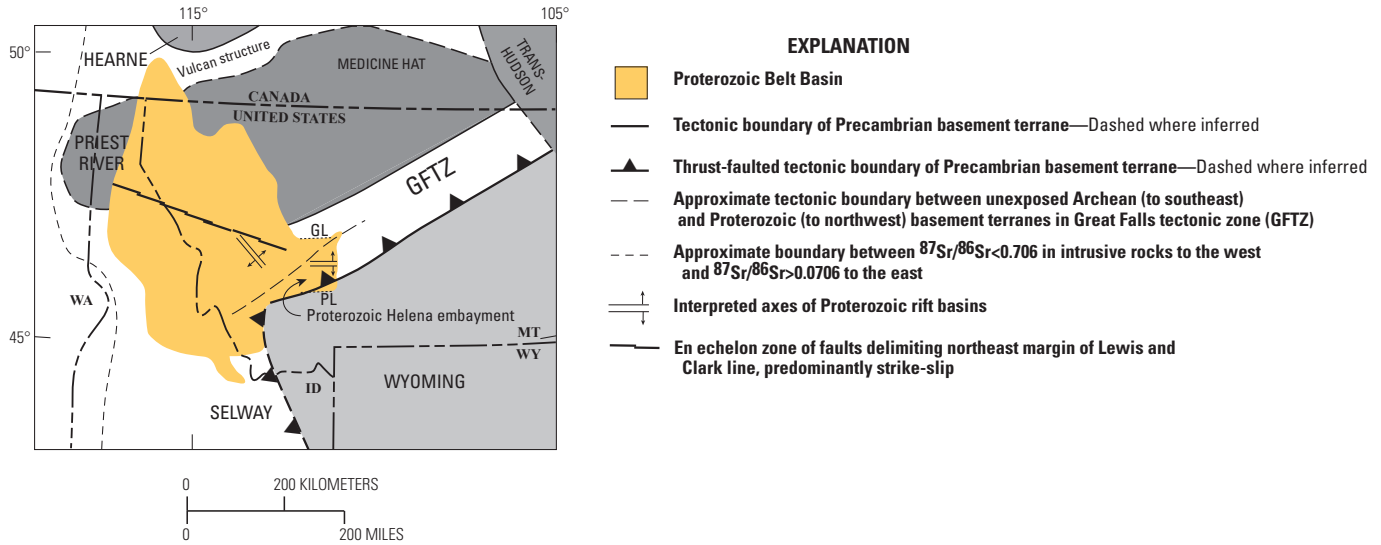
Figure 4.   Outline of the Belt Basin on a part of the basement terrane map shown in figure 1. The figure also shows the orientations of normal faults that were active across the basin during its development, the northeast margin of the Lewis and Clark line, the margins of the Great Falls tectonic zone (GFTZ), the projection of the main suture between the Archean Wyoming block to the southeast and the Proterozoic Medicine Hat block to the northwest, and the location of the northern and southern structural margins of the Helena embayment. These structural zones are known by various names including the Garnet line (GL) in the north and the Perry line (PL) in the south.
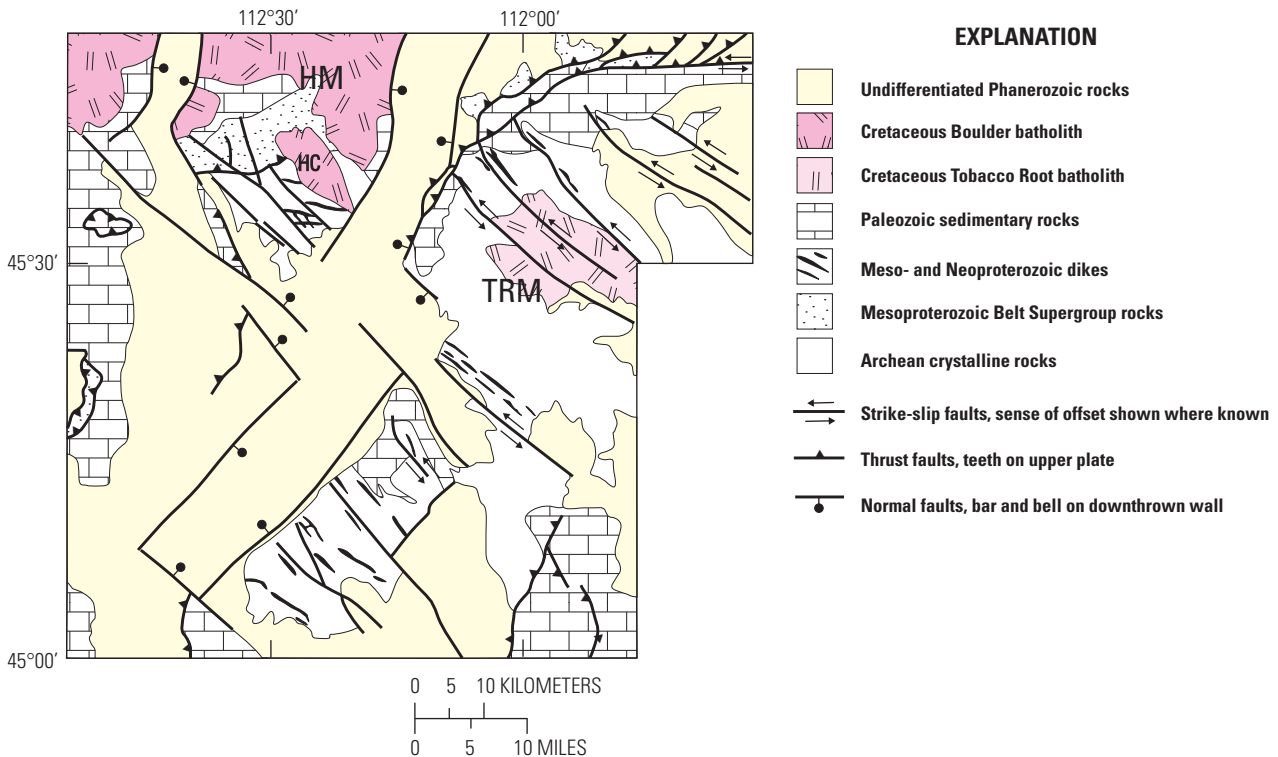
Figure 5.   Generalized geologic map of a part of the Highland Mountains (HM) at the southern end of the Boulder batholith. The Hell Canyon pluton (HC) and Tobacco Root Mountains (TRM) are shown for reference. Mesoproterozoic and Neoproterozoic dikes are shown in black. As mapped, the northwest-striking left-lateral faults are a Mesozoic reactivation of originally Mesoproterozoic normal faults (after Harlan and others, 1996).
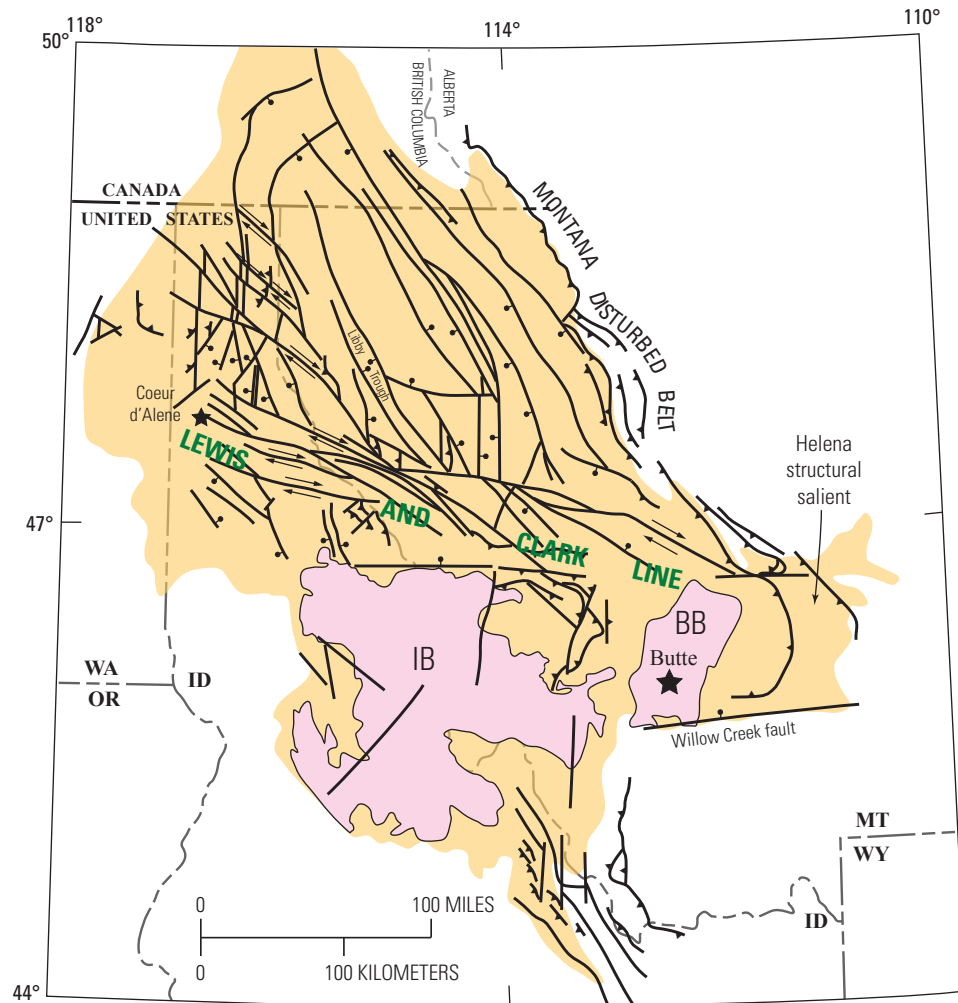
Figure 6. Generalized tectonic map of southwestern Montana during the Late Cretaceous showing the principal thrust-fault complexes, regional-scale faults, and locations of the Proterozic Belt Basin and Cretaceous batholithic complexes. The Cretaceous Montana disturbed belt corresponds with the northeast margin of the Belt Basin, and the Helena structural salient approximately corresponds to the Helena embayment of the Belt Basin. The region of deformation known as the Lewis and Clark line is shown for reference (BB, Boulder batholith; IB, Idaho batholith; after Harrison, 1972).
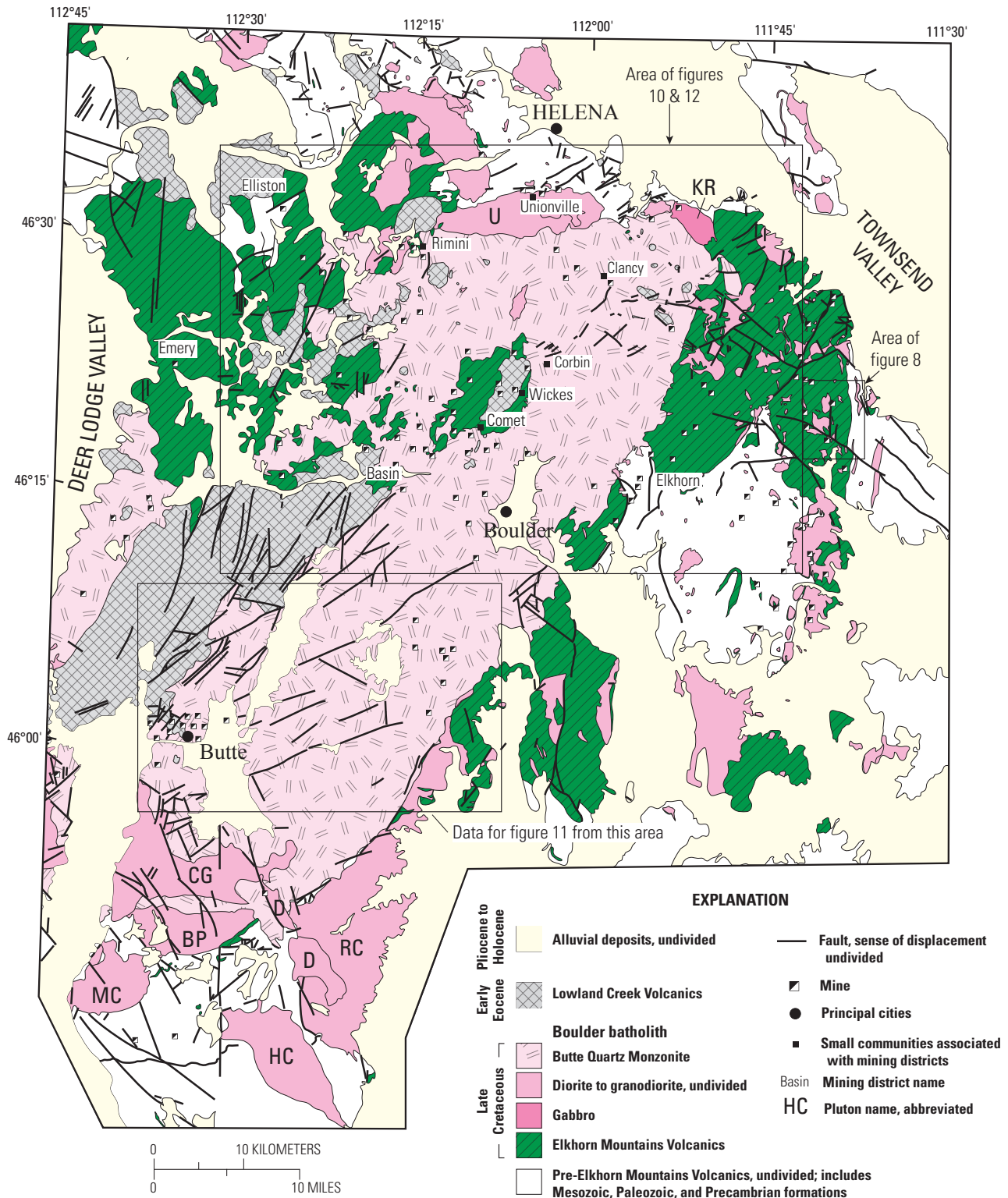
Figure 7.   Generalized geologic map of the Boulder batholith. Individual plutons labeled are Burton Park (BP), Climax Gulch (CG), Donald (D), Hell Canyon (HC), Kokoruda Ranch Complex (KR), Moose Creek (MC), Rader Creek Granodiorite (RC), and Unionville Granodiorite (U). Black circles denote locations of major cities in the area, black squares denote locations of selected mining districts, and the general distribution of mines is indicated by the black and white shaft symbols (after Klepper and others, 1957; Becraft and others, 1963; Knopf, 1963; Ruppel, 1963; Prostka, 1966; Smedes, 1966, 1967, 1968; Klepper and others, 1971b).
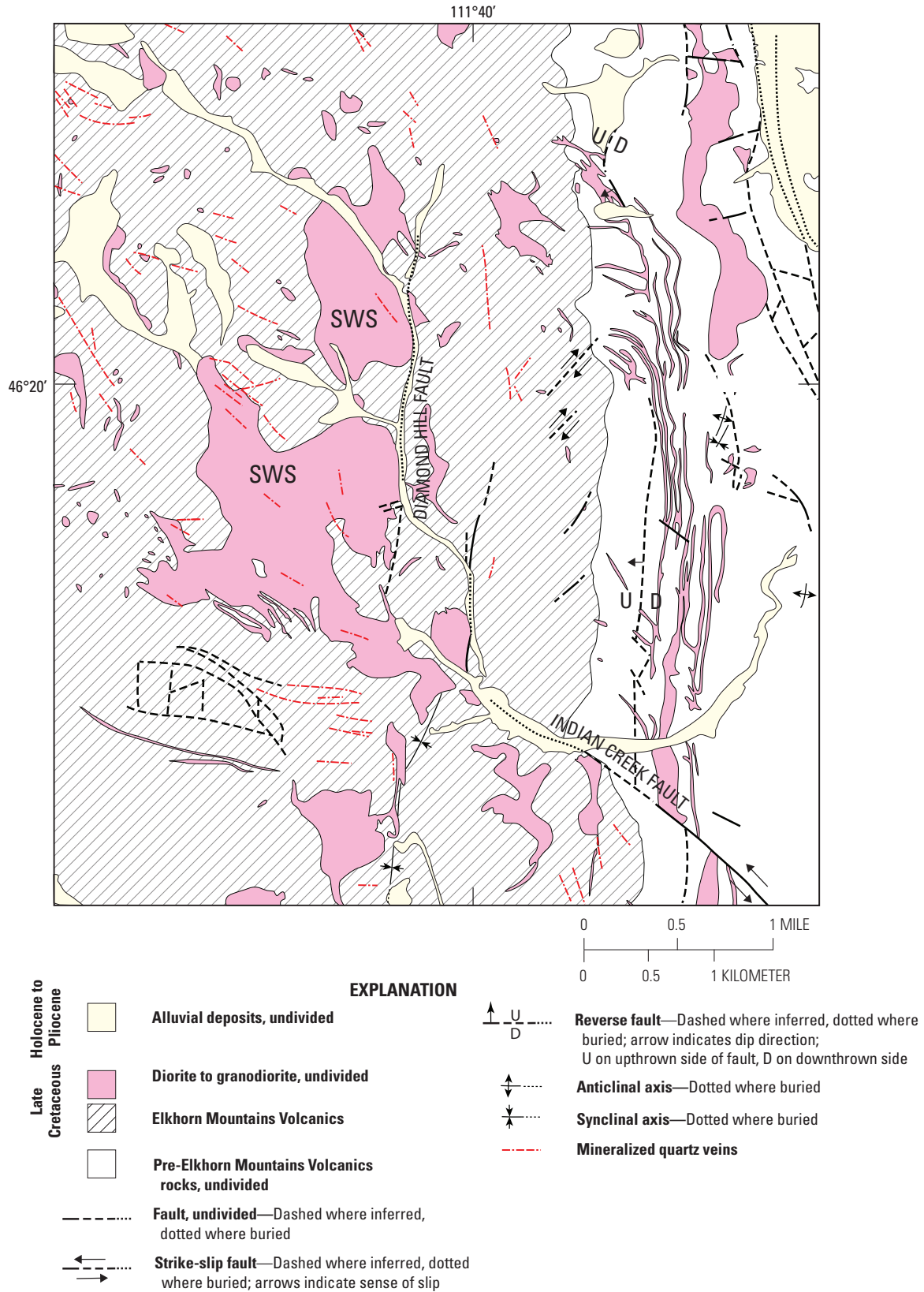
Figure 8.   Generalized geologic map of a part of the east margin of the Boulder batholith showing the relation of (1) early-stage sills to north-striking reverse faults and intrusions and (2) related quartz-sulfide veins to northwest-striking strike-slip faults (SWS, Silver Wave stock; after Klepper and others, 1971b).

elongated northwest-southeast, and, in the Hell Canyon stock, Tilling (1968) mapped discrete compositional zones whose long axes parallel the margins of the stock. Thus, field relations are indicative of a temporal evolution during early-stage magmatism from west-dipping reverse faulting to strike-slip accommodation of shear in the vicinity of the batholith.

The Precambrian heritage of the northwest-striking faults that localized early stage plutons is circumstantial, but the spatial correlation of the Hell Canyon pluton (fig. 7) and Precambrian faults and dikes (fig. 5) is permissive and supported by geophysical data. Linear trends in the regional gravity and magnetic data defined after removal of those correlating with topographic trends strike almost exclusively northwest (fig. 9). Some of these may be traced laterally into mapped Proterozoic faults in exposed basement rocks. Therefore, we assume that most northwest-trending basement lineaments throughout the mapped area are reflective of Proterozoic basement deformation.

There are a number of sill complexes along the west margin of the batholith that have been interpreted previously as indicating that the west margin of the batholith is laccolithic (for example, Lawson, 1914; Schmidt and others, 1990; O'Neill and others, 2004). As discussed below, the potential field data do not support the laccolith hypothesis, and we interpret the sills on the west side of the batholith as analogous to synthrust fault-related sills on the east and north margins of the batholith.

Tectonic and Structural Localization of Later-Stage Magmas

Although the later-stage intrusions are texturally heterogeneous, they are sufficiently homogeneous in composition to render their contacts generally indistinguishable in the field. As a consequence, excepting the Climax Gulch pluton (fig. 7), the later-stage intrusions are mapped as a single unit, the Butte Quartz Monzonite. In contrast to the irregular geometries of the early stage plutons, the Butte Quartz Monzonite is a remarkably symmetric mass with parallel north and south as well as east and west margins. The long, northeast-trending axis of the pluton is 90 km long, and it is about 50 km wide. The Butte Quartz Monzonite generally has a flat contact with its roof rocks (Hamilton and Myers, 1967).

Younger rocks mask the western margin of the Butte Quartz Monzonite, but the other boundaries are sufficiently well exposed to provide information regarding structural controls along the margins. Along the southeast margin of the Butte pluton, Prostka (1966) mapped a contact-parallel and commonly vertical shear fabric in an early-stage diorite and the overlying Elkhorn Mountains Volcanics that is truncated by the Butte Quartz Monzonite. Along the same contact farther southwest, there is a screen of pre-Mesozoic rocks between the Butte Quartz Monzonite and the early-stage Rader Creek Granodiorite pluton (fig. 7). Some beds within these sedimentary rocks are vertical to overturned against the contact

(Klepper and others, 1971a). Also along the east boundary, Schmidt and others (1990) report that mafic enclaves are abundant and the enclaves are flattened parallel to the pluton margin. Adjacent to the margin, there is commonly also a foliation fabric in the pluton parallel to the enclaves. Schmidt and O'Neill (1982) and Schmidt and others (1990) interpret the above fabrics as thrust-fault related and evidence that the east margin of the Butte Quartz Monzonite is structural and follows the trace of a pre–Butte Quartz Monzonite thrust fault.

Late-Stage Dikes and Veins

With the exception of the earliest magmas, the Boulder batholith plutons postdate thrust faulting; farther east and north, the frontal thrust zone was active into the Paleocene (Mehnert and Schmidt, 1971; Harlan and others, 1988). Thus, for the duration of batholith emplacement, the entire region was under compression with the maximum principal stress horizontal and oriented east-west, a condition that persisted through the Paleocene.

The final stage of the Butte Quartz Monzonite magmatism consists of the emplacement of numerous pegmatite, alaskite, and aplite dikes (fig. 10). Detailed mapping of dikes (Becraft and others, 1963; Ruppel, 1963; Smedes, 1966; Houston, 2002) provides insights regarding the state of stress that controlled fluid flow during the final emplacement of Butte Quartz Monzonite magmas. Figures 10 and 11 show rose diagrams of dike orientations of Butte Quartz Monzonite dikes as well as early stage dikes in the northeast part of the batholith. Within the Butte Quartz Monzonite, a preferred northeast orientation contrasts with the more equally distributed northeast and northwest orientations exhibited by dikes associated with pre–Butte Quartz Monzonite, Boulder batholith intrusions. Most of the analyzed dikes crop out within a 4- to 6-km-wide northeast-trending corridor that extends obliquely across the entirety of the pluton. Near Butte, in the southern part of the batholith and in contrast to the northern part of the batholith, there is a strong, generally east-west pattern evident in the dike orientations (fig. 11).

Immediately following the crystallization of the Butte Quartz Monzonite and related dikes, sulfide-bearing quartz veins were formed in the northern half of the Butte Quartz Monzonite (fig. 12) with a predominant east-west strike.

Geophysical Model of the Butte Quartz Monzonite

To obtain a three-dimensional (3D) image of the Boulder batholith and provide a context for interpreting mechanical controls on emplacement of the batholith, we synthesized magnetic, gravity, petrological, geochemical, and seismic data and applied modern interpretative techniques. Owing to the sharp density contrast between the lower density siliceous igneous rocks and their denser sedimentary and metamorphic
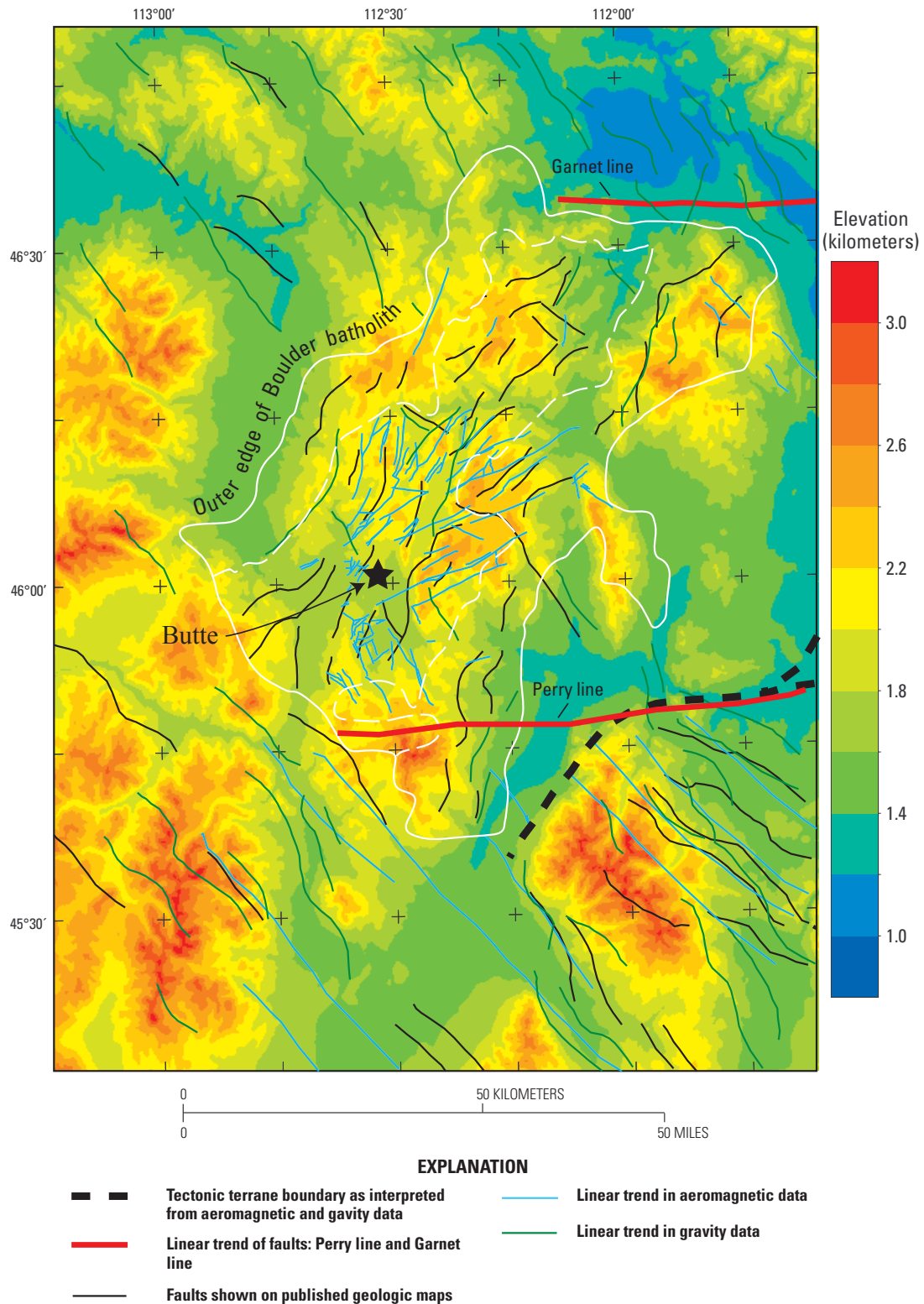
Figure 9.   Topographic map (highest elevations in red, lowest in blue) showing linear trends in the regional gravity and magnetic data defined after removal of those correlating with topographic trends. The outer, solid white line boundary delimits the geophysical margin of the Boulder batholith; the inner, dashed white line delimits the outer geophysical margin of the Butte Quartz Monzonite phase of the batholith. The location of the city of Butte (star) shown for reference.

EXPLANATION

Holocene to Pliocene	Alluvial deposits, undivided
Early Eocene	Lowland Creek Volcanics

Boulder batholith

Late Cretaceous
- Late-stage dikes, predominantly granite pegmatite and alaskite
- Butte Quartz Monzonite
- Diorite to granodiorite, undivided
- Gabbro
- Elkhorn Mountains Volcanics

Pre-Elkhorn Mountains Volcanics, undivided; includes Mesozoic, Paleozoic, and Precambrian formations

— Fault, undivided

● Principal city

Figure 10. The distribution and orientation of early- and late-stage aplite, pegmatite, and alaskite dikes on a generalized geologic map of the northern half of the Boulder batholith (after Becraft and others, 1963; Ruppel, 1963; Smedes, 1966). Inset rose diagrams *A* and *B* pertain to measured orientations of late-stage dikes in the Butte Quartz Monzonite pluton; *A*, measured outside of the outlined area; *B*, measured within the outlined area. Inset rose diagram *C* pertains to early-stage dikes measured within the outlined area.

host rocks, gravity data were used to determine the shape of the batholith. The lateral extent of the batholith beneath volcanic and surficial cover was determined from the analysis of magnetic data. Structural trends within and surrounding the batholith were highlighted through the filtering of the potential-field data. The inversion of gravity and magnetic data provided a base from which a 3D model and visualization of the Butte Quartz Monzonite could be constructed.

Geophysical Data and Modeling

A reduced-to-pole aeromagnetic map of the Boulder batholith and vicinity and a residual short-wavelength magnetic anomaly map of the same region are shown in figure 13. The magnetic data were extracted from a previously compiled digital dataset composed of several aeromagnetic surveys (McCafferty and others, 1998). Survey line spacing in the
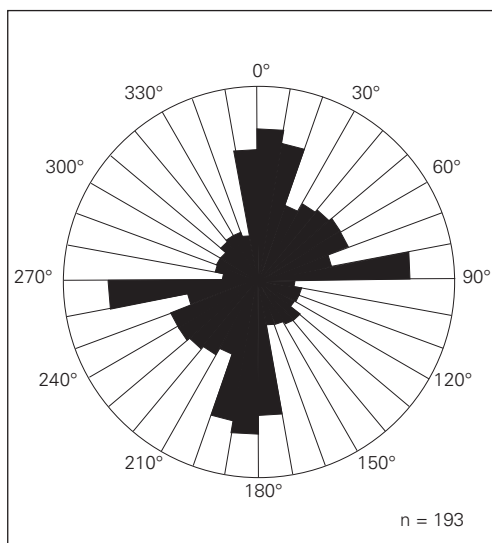
Figure 11. Rose diagram for late-stage dikes in the Butte Quartz Monzonite in the southern half of the batholith. The predominance of north-south and east-west orientations contrasts with preferred dike orientations in the northern half of the Butte Quartz Monzonite as shown in figure 10. The map area from which the orientation data were made is shown in figure 7 (after Smedes, 1967, 1968; Houston, 2002).

study area is 1.6 km or less, except in small areas in the extreme northeast and southeast corners of the area where the spacing is 3.2 km. A 1-km grid of magnetic values was prepared for each aeromagnetic survey using a minimum curvature algorithm (Webring, 1981). All data were analytically continued to a surface 305 meters (m) above the terrain. Assuming induced magnetization or remanent magnetization aligned or nearly aligned in the direction of Earth's magnetic field, the magnetic-anomaly data were reduced to the magnetic pole, a procedure that shifts magnetic anomalies to positions above their sources.

An isostatic gravity anomaly map of the Boulder batholith and vicinity and a residual short-wavelength gravity anomaly map of the same region are shown in figure 14. The gravity data were taken from the National Geophysical Data Center database (approx. 4,000 stations). All data were tied to the IGSN-71 gravity datum (International Gravity Standardization Net 1971) and reduced to complete terrain-corrected Bouguer-anomaly values using a reduction density of 2,670 kg/m^3 (kilogram per cubic meter) and the 1967 formula for the theoretical gravity of the Earth (Cordell and others, 1982). The spacing of gravity stations is generally adequate (about 1 station per 5.5 km^2) to define and characterize upper crustal features within the study area. A 1-km grid of gravity values was prepared using the Webring (1981) algorithm. To

compensate for the load on the crust caused by the additional mass of mountains, the isostatic residual gravity anomaly was determined (Simpson and others, 1986), which reflects more closely the contribution of intracrustal density variations.

The complex magnetic and gravity patterns shown in figures 13 and 14 indicate anomalies from a variety of sources lying at different depths. This superposition of anomalies can result in interpretational ambiguities. To locate near-surface magnetic and gravity sources, regional anomalies were first removed to isolate short-wavelength anomalies of interest (the residual maps), and then horizontal-gradient analysis aided in locating the edges of these sources (the small circles on residual maps). The magnetic and gravity data were continued upward analytically 1 km to generate regional fields. These regional or low-frequency-passed fields were then subtracted from the unfiltered dataset to derive the residual or high-frequency-passed fields. Combining the unfiltered and residual magnetic data in this manner highlights subtle geologic information for different depths. Several linear geophysical features became apparent.

Two filtering approaches were used to enhance geophysical boundaries. The first method employs horizontal gradient analysis, which is an analytical mapping tool that defines interpreted rock-unit boundaries and their orientation on the basis of local curvature of the magnetic potential field or gravity field (Grauch and Cordell, 1987). Maxima in the horizontal gradient of these fields occur near steep boundaries separating contrasting magnetizations or densities. The locations of high horizontal gradients, automatically determined (Blakely and Simpson, 1986), are shown in figures 13*B* and 14*B* as the alignment of very small black circles. In the second method, a shaded-relief filter was applied to the residual magnetic data to further enhance magnetization boundaries.

Before applying a 3D modeling technique, a two-dimensional (2D) modeling program based on Webring (1985) was used to understand the lateral variations of total magnetization and density along ten selected profiles shown in figures 13*A* and 14*A*, respectively. In the modeling process, the bodies are assumed to extend a specified distance normal to the profile. The program uses nonlinear inversion and requires an initial estimate of model parameters including depth, shape, density, and total magnetization of suspected terranes. The program adjusts the values of selected parameters such that the weighted root mean square errors are minimized between the observed and calculated magnetic and gravity fields. The interpretation of either magnetic or gravity data yields non-unique solutions because a large number of geometric models will have an associated field that closely matches the measured field. In the derivation of a suitable geophysical model to represent the geologic setting of the Boulder batholith, drill-hole information, physical property data, seismic interpretations, and sound geologic reasoning were used.

To translate observed magnetic and gravity anomalies into a 3D geologic picture of the subsurface, we used an inverse modeling computer algorithm (Cordell and Henderson, 1968) that solves for the thickness of a density layer with
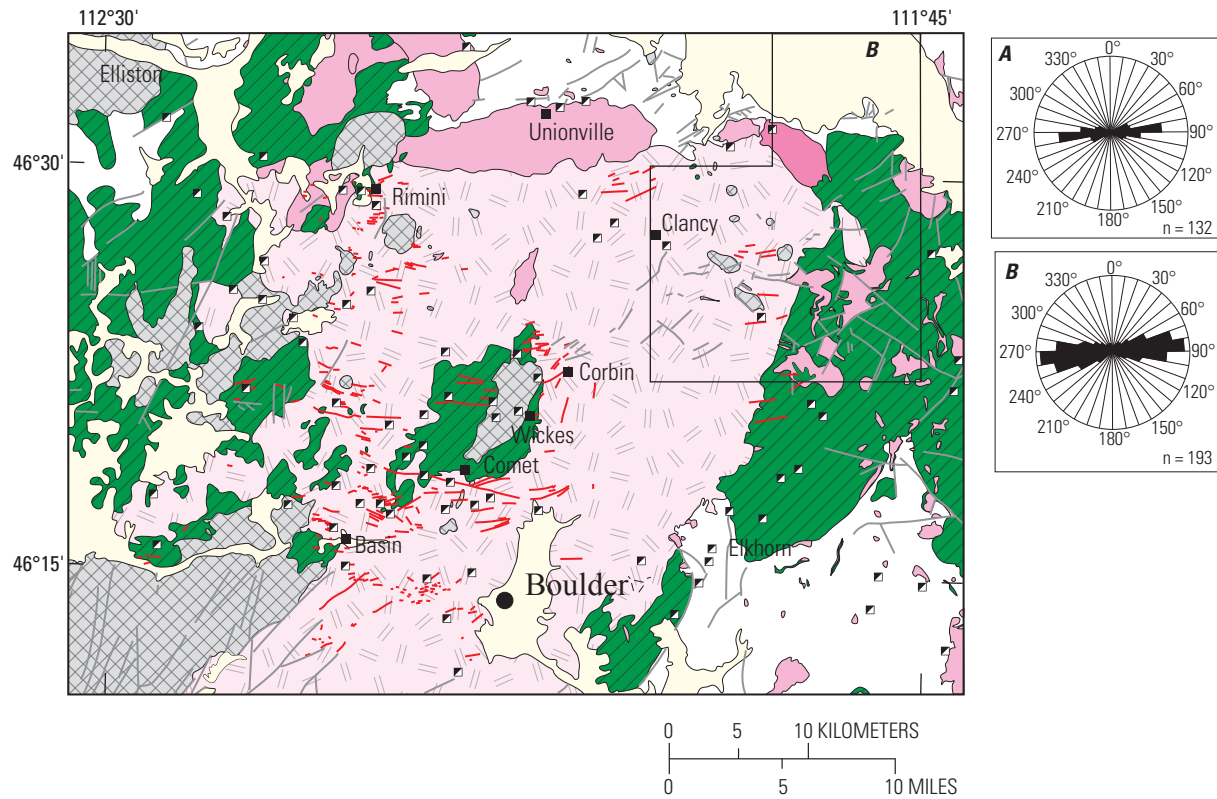
Figure 12.   The distribution and orientation of latest-stage sulfide-bearing quartz veins on a generalized geologic map of the northern half of the Boulder batholith. *A*, Inset rose diagram pertaining to orientations measured outside of the outlined area; *B*, Inset rose diagram pertaining to orientations measured within the outlined area (after Becraft and others, 1963; Ruppel, 1963; Smedes, 1966).
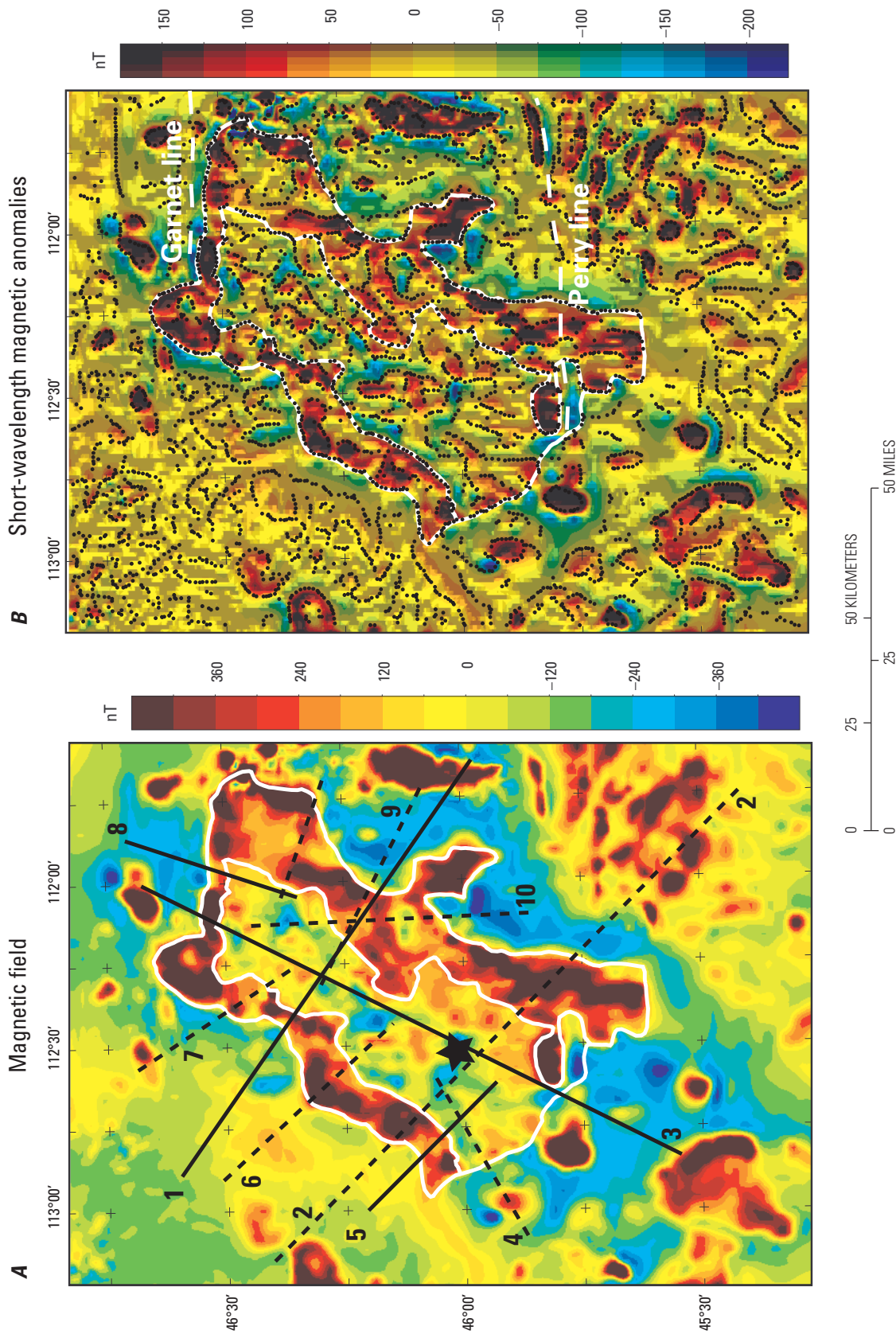
Figure 13.   Reduced-to-pole aeromagnetic maps of the Boulder batholith and vicinity. The outer bold white line is the interpreted outer geophysical margin of the batholith. The inner bold white line is the interpreted outer geophysical margin of the Butte Quartz Monzonite. (nT, nanotesla) *A*, Reduced-to-pole aeromagnetic map. The numbered black lines show the locations of profiles used to model the batholith. Solid black lines (1, 3, 5, 8) indicate those profiles shown in figure 16. The location of the Butte mining district is shown by a star symbol. *B*, Aeromagnetic map based on the shorter wavelength portion of the spectrum to emphasize shallow features. The small dots are inflection points in the magnetic wave forms. Lines of small dots are interpreted as boundaries between rocks with differing physical properties. The bold white dashed lines indicate the locations of the Garnet line and Perry line, shown for reference.
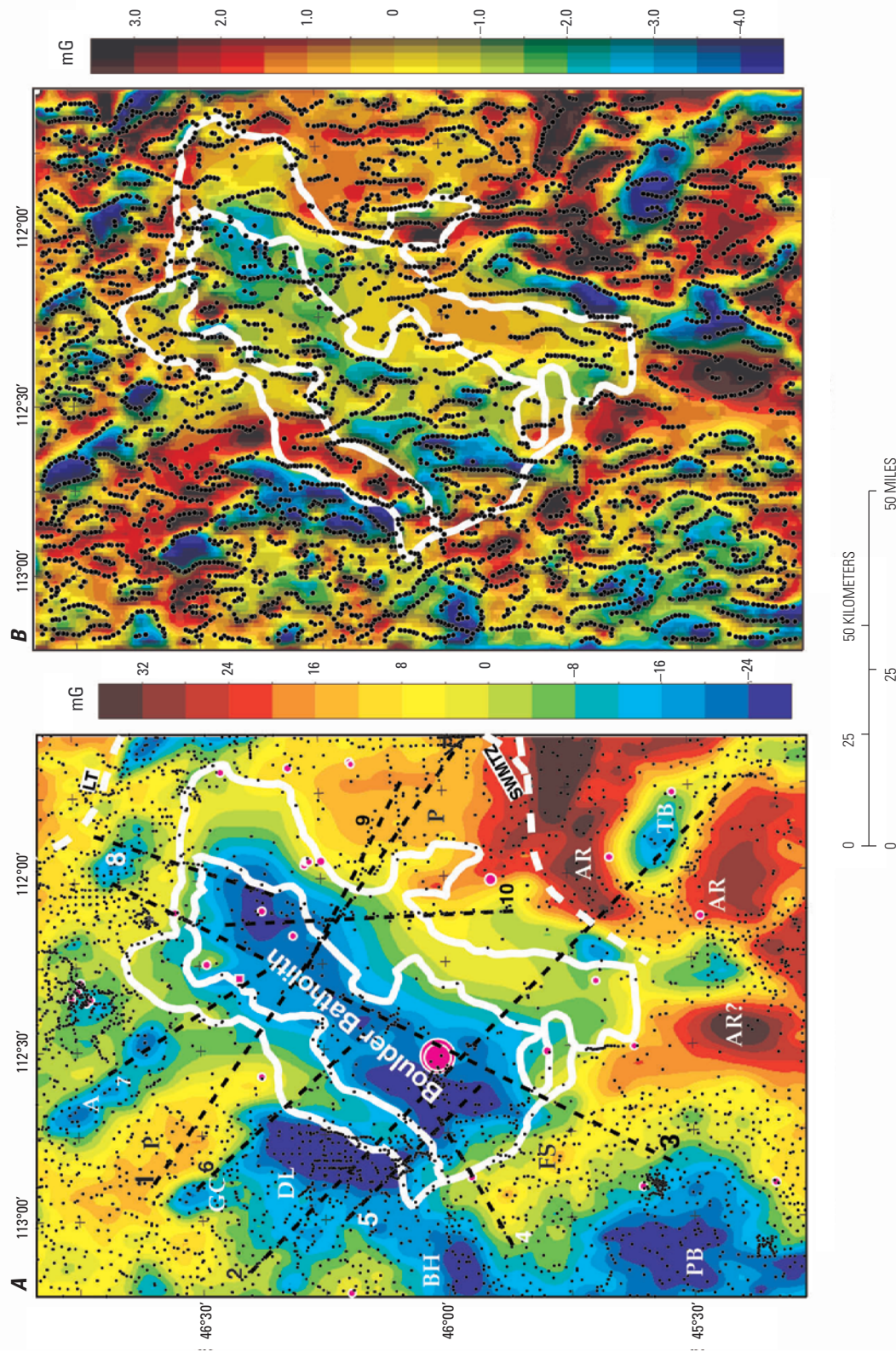
Figure 14.   Gravity maps of the Boulder batholith and vicinity. The outer bold white line is the interpreted outer geophysical margin of the batholith. The inner bold white line is the interpreted outer geophysical margin of the Butte Quartz Monzonite. (mG, milligal) *A*, Isostatic gravity anomaly map. The numbered dashed black lines show the locations of profiles used to model the batholith. Larger numbers (1, 3, 5, 8) indicate those profiles shown in figure 16. The bold white dashed lines are major tectonic lineaments: Lombard thrust (LT) and southwest Montana tectonic zone (SWMTZ). Mining localities documented in the U.S. Geological Survey's Mineral Resource Data Base are shown with pink-filled circles. Black dots are data collection sites. The interpretation of sources for the major anomalies are abbreviated as follows: A, Avon; AR, Archean rocks; BH, Big Hole Valley; FL, Fleecer Stock; GC, Clark Fork River valley; DL, Deer Lodge Valley; PB, Pioneer batholith; P, Proterozoic Belt Basin rocks; and TB, Tobacco Root batholith. *B*, Residual isostatic gravity anomaly map. The small dots are inflection points in the magnetic wave forms. Lines of small dots are interpreted as boundaries between rocks of differing physical properties.

a specified flat upper surface, herein selected as the mean topographic elevation. The gravity field in the vicinity of the Boulder batholith and a density contrast of 150 kg/m³ between the batholith and surrounding country rocks were used. Because rock density varies along the flanks of the batholith, as suggested in the 2D models, the assumption of uniform density contrasts may locally be much greater than 150 kg/m³. Thus, the calculated values in the 3D model are moderately unconstrained and only the relative changes in the thickness should be considered and interpreted as major changes in the bulk mass properties of the batholith.

Results of Geophysical Data Analysis

The magnetic data (fig. 13) primarily reflect isolated plutons or clusters of plutons, as well as magnetization variations in Cretaceous and Eocene volcanic fields and the plutonic rocks (fig. 7). The outer boundary of the Boulder batholith is clearly defined by a magnetic boundary (fig. 13A) separating pronounced positive anomalies over the more mafic plutons of the batholith from lower intensity anomalies lying outside the batholith. The magnetic highs associated with the early-stage plutons form a remarkable, symmetrical ring around the late-stage Butte Quartz Monzonite. Magnetic expression of the ring is absent only in a short segment along the southwest edge of the batholith. The inner edge of the ring (fig. 13A) is the Butte Quartz Monzonite. The Butte Quartz Monzonite is reflected in much lower intensities in the magnetic (fig. 13) and gravity (fig. 14) fields. About halfway from the northern to southern boundaries of the Butte Quartz Monzonite, the outer higher intensity magnetic ring correlative with the early-stage plutons appears on both sides of the batholith to indent the center of the batholith (fig. 13A). This geometry is suggestive that there may be two separate lobes of the Butte Quartz Monzonite that coalesced across the top of underlying early-stage intrusions not wholly evident in the potential-field data.

The gravity data delineate the major rock types in the study area. Primarily low-density basin fill, plutons, and volcanic rocks form prominent gravity lows (fig. 14A) in contrast to denser Paleozoic and Precambrian rocks. Low-density volcanic and plutonic rocks associated with the Boulder batholith are delineated by a pronounced northeast-trending negative gravity anomaly. Similar gravity lows in the southwest (PB in fig. 14A) and southeast (TB in fig. 14A) corners of the map are the edges of Late Cretaceous batholiths. Prominent gravity highs generally occur over dense plutons and Archean and Paleoproterozoic rocks such as mafic gneiss, amphibolite, and iron formation, particularly south of the southwest Montana tectonic zone (SWMTZ in fig. 14A). Less intense gravity highs overlie moderately dense Paleozoic and Mesoproterozoic sedimentary rocks.

Spectral inversion of magnetic and gravity data within a 120-km² area centered on the batholith required a three-layer model to properly fit or model the radial amplitude spectra of both magnetic and isostatic gravity data within and external to the margins of the batholith. The top layer is less than 1.3 km deep and is probably related primarily to the noise and errors within the datasets. Outside the boundary of the batholith, the second layer is at depths of 3.3 km and 2.8 km below the ground surface based on the spectrum of magnetic and gravity data, respectively. These depths are likely related to a combination of sources lying roughly, for example, at the average depth of pre-Mesoproterozoic metamorphic rocks or the base of volcanic fields. Within the batholith, the calculated depths of the third layer from the magnetic and gravity data are 5.9 km and 5.4 km below the surface based on the spectrum of magnetic and gravity data, respectively. We interpret the resulting average of 5.7 km to approximate the thickness of the batholith.

Figures 13A and 14A show the locations of the profiles used in the 2D modeling. Model results for profiles 1 and 5 are shown in figure 15 and for profiles 3 and 8 in figure 16. In the initial model, the bottoms of the upper crustal layer and of the batholith defined in the spectral analysis were assumed to be 1.2 km and 4 km below sea level, respectively. However, this assumption did not produce acceptable results for the assumed densities of basin fill (2,200 kg/m³), Butte Quartz Monzonite (2,670 kg/m³), and the middle crustal layer (2,820 kg/m³). Therefore, along most profiles, it was necessary to increase the depth of the bottom of the upper crustal layer to about 3 km below sea level and of the batholith to about 6 km below sea level. Thus, for the assumed densities, the batholith thickness is approximately 7.8 km.

Profiles 1 (fig. 15A) and 3 (fig. 16A) cross the entire batholith, while profiles 5 (fig. 15B) and 8 (fig. 16B) cross only an edge of the batholith. The calculated fields of the simple sources that are shown reasonably match the observed fields. Analogous to its outcrop shape, the batholith is also a remarkably uniform rhombohedral shape in 3D. The outer contact of the batholith is nearly vertical in all studied profiles, whereas the boundaries between the early-stage, moderately to strongly magnetic (1.1–2.3 A/m [ampere-turn per meter]), and dense (2,680–2,770 kg/m³) plutons and the Butte Quartz Monzonite (1 A/m and 2,670 kg/m³) dip inward from 15° to 82° and, most commonly, between 45° and 60°. Along profile 3 (fig. 15B), the strong magnetic source (2.3 A/m) in the outer ring at the north end of the batholith corresponds with an east-west–elongated pluton known as the Unionville Granodiorite (2.3–5.2 A/m) (fig. 7).

The topography of the basal surface of the Butte Quartz Monzonite derived in 3D modeling from a grid of vertical rectangular prisms is depicted in figure 17. The walls of the pluton dip inward to a generally flat bottom at 6- to 8-km depth. Towards the north-central and south-central ends of the batholith, there are two zones with calculated depths of 13–15 km. This overall geometry suggests that the Butte Quartz Monzonite magma was fed from depth principally through two separate zones at the base of the batholith. Thus, overall, the plan outline of the Butte Quartz Monzonite (fig. 7) is a composite of two funnel-shaped masses. The boundary of the two zones is interpreted to be where there are re-entrants
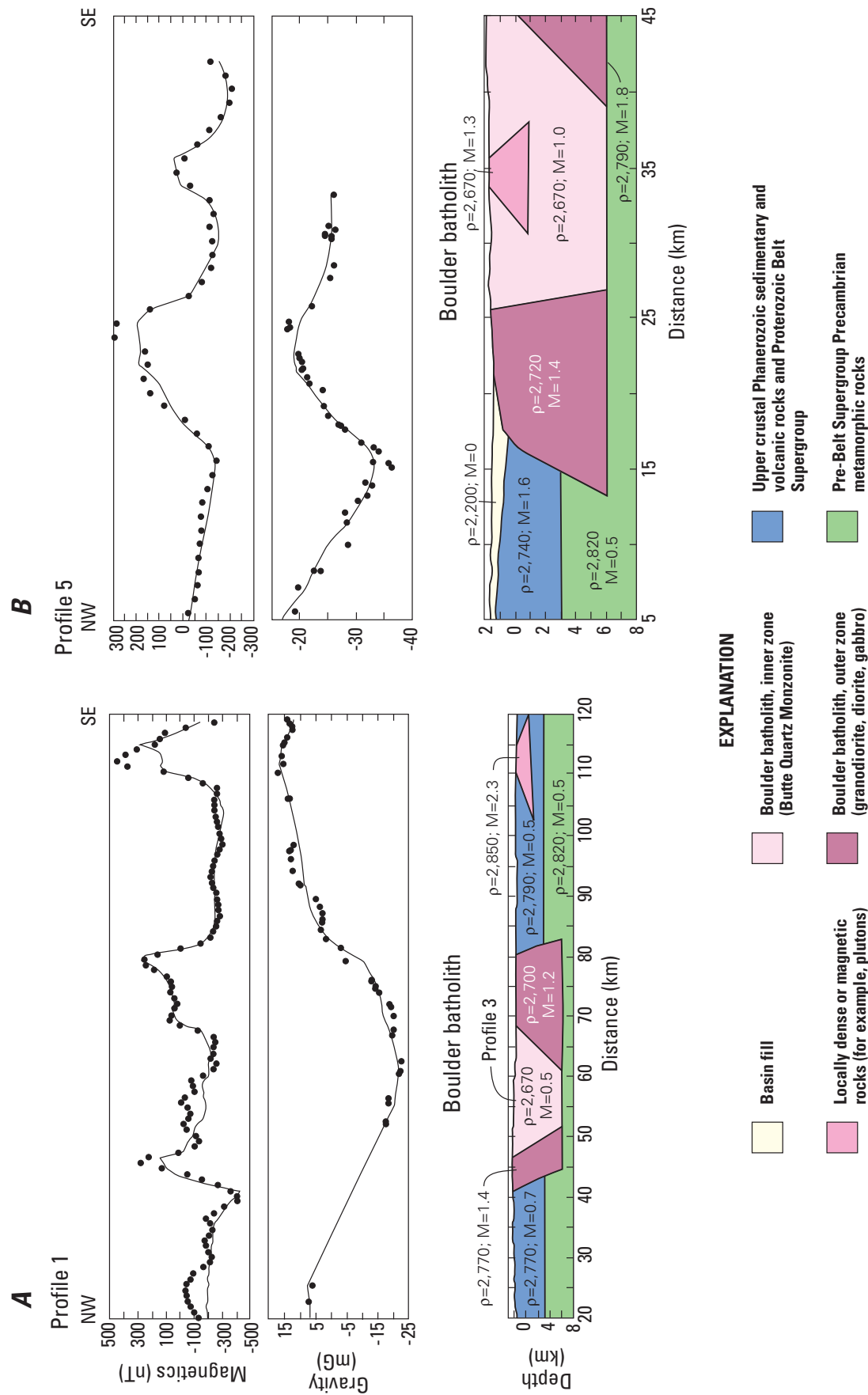
Figure 15. Simultaneous inversion of magnetic and actual magnetic and gravity fields (upper diagrams) and 2D model (lower diagram) for profiles 1 and 5. Locations of modeled profiles are shown in figures 13A and 14A. *A*, Profile 1 is a northwest-southeast cross section across the northern part of the batholith. *B*, Profile 5 is a section across the southwestern edge of the batholith. (ρ, rock density; M, magnetic susceptibility; nT, nanotesla; mG, milligal; km, kilometer).
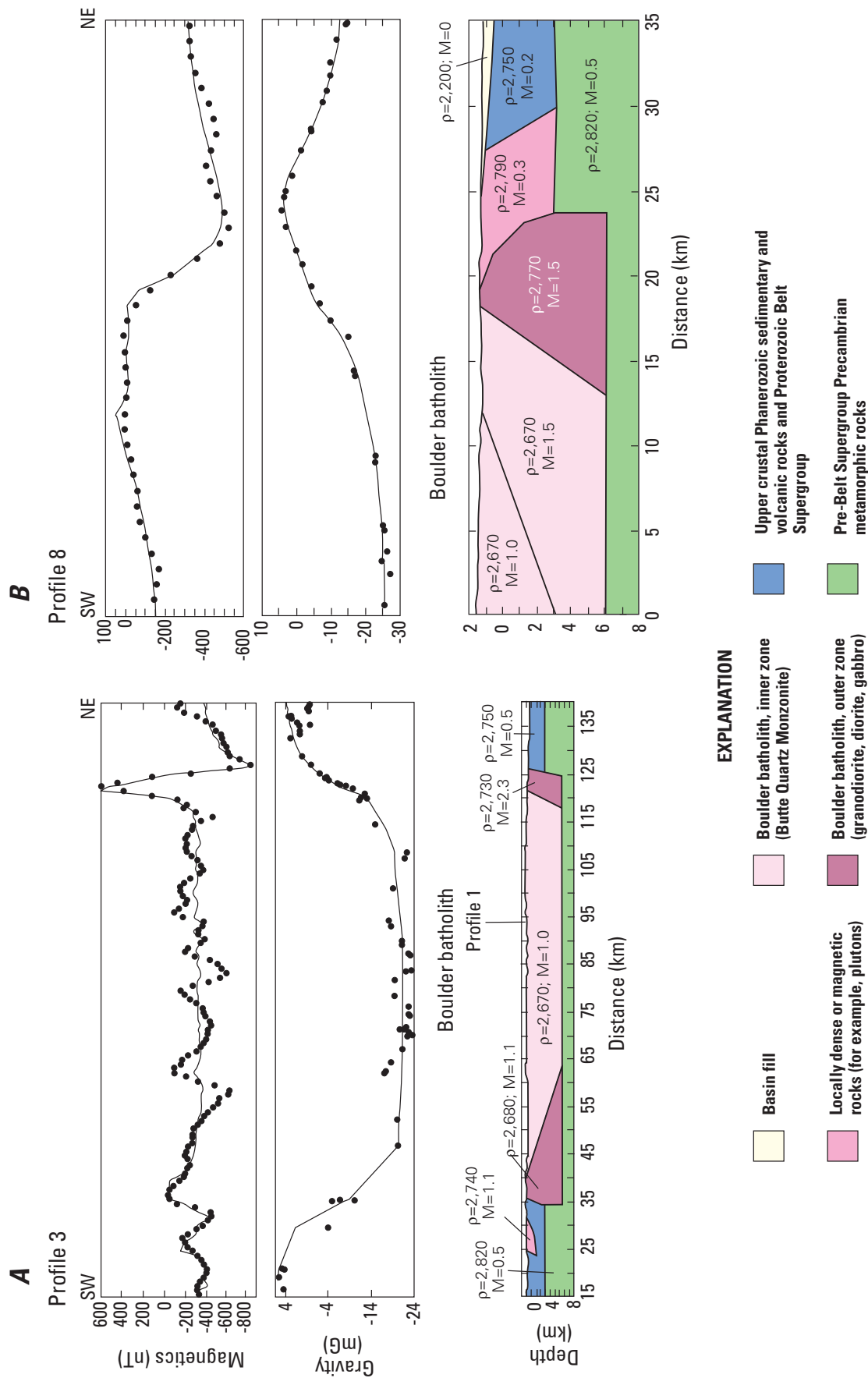
Figure 16. Simultaneous inversion of magnetic and gravity data across the Boulder batholith showing computed and actual magnetic and gravity fields (upper diagrams) and 2D model (lower diagram) for profiles 3 and 8. Locations of modeled profiles are shown in Figures 13A and 14A. *A*, Profile 3 is a southwest-northeast profile through the Butte mining district across the center of the batholith. *B*, Profile 8 is a section across the northeastern edge of the batholith. (ρ, rock density; M, magnetic susceptibility; nT, nanotesla; mG, milligal; km, kilometer).
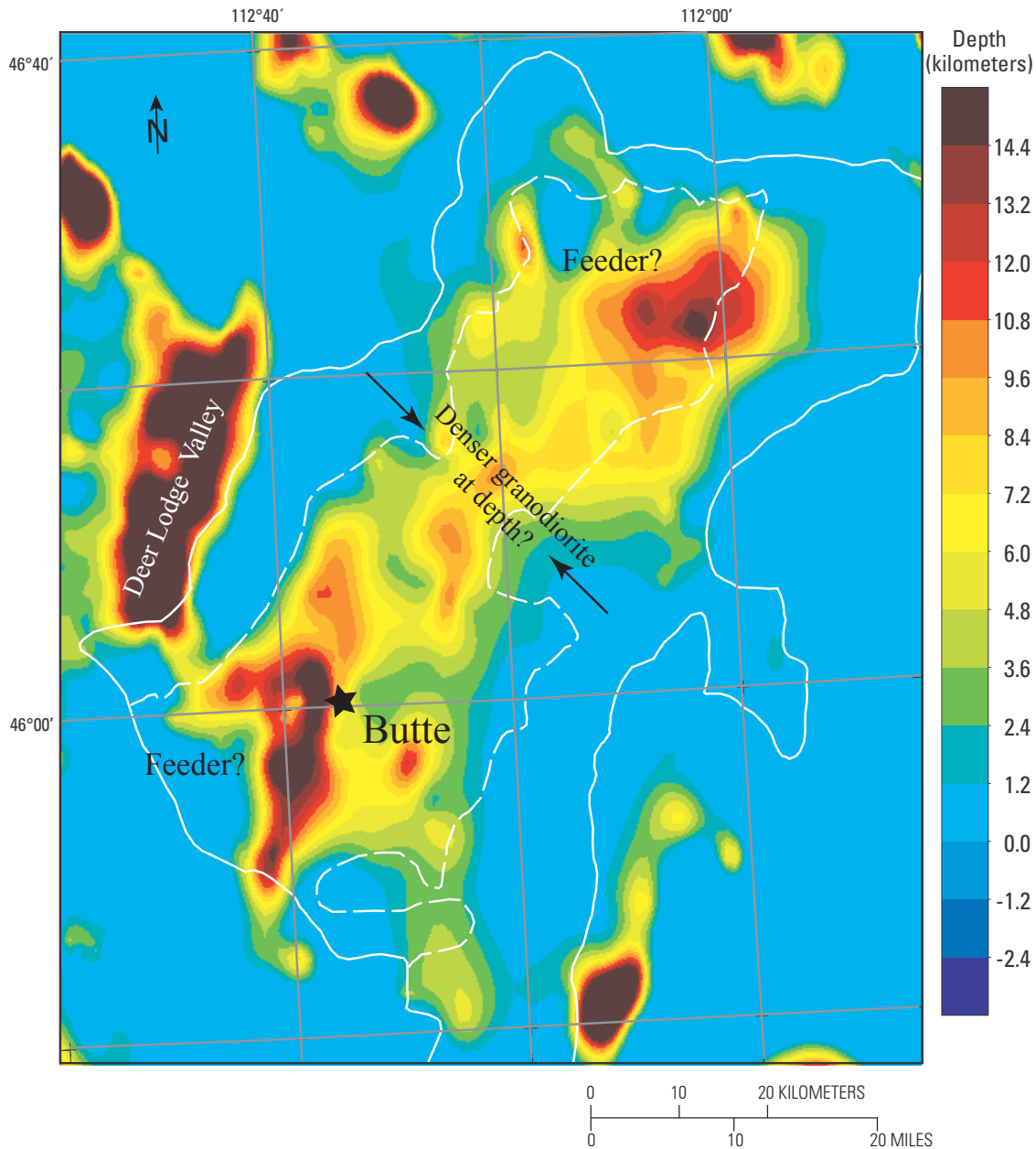
Figure 17.   Contour map of calculated depths to the base of the Butte Quartz Monzonite using a 3D gravity inversion model. The average modeled depth of the base is 6 kilometers (km). The floor rapidly descends to depths exceeding 10 km in two areas interpreted to be feeder zones for the Butte Quartz Monzonite. The solid white line shows the geophysical outer boundary of the Boulder batholith; the inner dashed white line shows the geophysical outer boundary of the Butte Quartz Monzonite. The arrows indicate where the base of the batholith appears to pinch inward coincident with higher density batholithic rocks as indicated by magnetic data (see fig. 13*A*). The anomaly associated with the Deer Lodge Valley is a modeling edge effect.

into the Butte Quartz Monzonite of more magnetic (fig. 13*A*) and denser, early-stage intrusions. The rings of denser igneous material may be continuous at depth, but the available data are inadequate to address this issue.

The total volume of the batholith is difficult to calculate. As noted previously, different modeling assumptions and approaches give different estimates of the thickness of the batholith. In studying 21 plutons with thicknesses geologically known or determined from geophysical studies, McCaffrey and Petford (1997) show that plutons have a horizontal dimension (*L*) greater than their thickness (*T*), which conforms to a relationship based on a power law:

$$T = 0.12 \, L^{0.88}.$$

Although erroneous estimates of thickness are anticipated in some situations using this equation, it leads to a reasonable value of 6.9 km for the Boulder batholith. Based on this result and the different modeling results, we estimate that the base of the Boulder batholith is likely deeper than 5 km and shallower than 10 km. Assuming a thickness of 7 km, the volume of the batholith is approximately 35,000 km³.

The Paleocene Butte Mining District

A 10-million-year (m.y.) hiatus followed emplacement of the Butte Quartz Monzonite before intrusive activity began again at 66–65 Ma (Lund and others, 2002) in the vicinity of Butte, Mont. East-west-striking and west-northwest-striking Paleocene quartz porphyry dikes crop out in the heart of the Butte district and in the mountains to the east. Presumed to reflect the presence of an east-west fracture zone in the district, the dikes were intruded on the eastern edge of the interpreted southern feeder zone for the Butte Quartz Monzonite. Paragenetically early porphyry-style copper-molybdenum and later polymetallic-vein deposits in the Butte mining district were formed 64–63 Ma (Snee and others, 1999; Lund and others, 2002). The deposits are hosted in the Butte Quartz Monzonite above the inferred southern feeder zone. There are two styles of polymetallic vein mineralization. One contains predominantly silver, lead, zinc, and subordinate copper ores with a gangue of quartz, pyrite, K-feldspar, calcite, sericite, and chlorite. The second contains predominantly copper, with subordinate zinc, silver, and lead, with a gangue of quartz, sericite, and pyrophyllite. Since 1880, the district has produced in excess of 9.2 megaton (Mt) of copper, 2.5 Mt of zinc, 439 kiloton (kt) of lead, 679 megaounce (Moz) of silver, and 2.8 Moz of gold (Miller, 1973).

The Butte mining district is localized in a complex, northeast-striking system of right-lateral and related faults (fig. 18). The fault patterns shown in figure 18 reflect vein-controlling structures (see Sales, 1914; Meyer and others, 1968). Short-dashed lines outline the locations of two porphyry-style deposits that underlie the vein systems. Traditionally, the intersections of different fault-vein orientations have been

used to classify the vein systems (for example, Sales, 1914). Based on apparent offsets, east-west faults (referred to as "Anaconda" system by Sales, 1914) were interpreted as earliest. They typically display normal-sense displacement. Northwest-striking faults (referred to as "Blue" system by Sales, 1914) followed. Blue system faults display left-lateral to left-lateral-oblique senses of displacement. Northeast to east-northeast faults (referred to as "Steward" system by Sales, 1914) were interpreted as youngest. Steward system faults have a right-lateral sense of displacement. Weed (1912) and Sales (1914) noted inconsistencies in this classification scheme in that not all faults within a given system are exactly the same age, and faults in an interpreted younger system of faults are sometimes offset by faults interpreted to be an older system of faults. Despite such inconsistencies, this three-part classification continues to be widely accepted (for example, Lund and others, 2002).

Based on several observations, we propose a different interpretation of how the fault systems in the Butte mining district formed and evolved.

1. As Sales (1914) noted, we observe that the northeast-to north-northeast–striking Steward faults are seldom offset by mineralized faults of other orientations, and they are the most continuous along strike.

2. Across the whole of the productive part of the district, with respect to the Steward faults, fault-veins of the Anaconda system have a mean splay angle of 25°±10° (n=29), and Blue system veins have a mean splay angle of 71°±9° (n=66), indicating a great deal of consistency in the fault systematics.

3. Each of the major Steward faults bends progressively clockwise, that is extensionally, along strike to form a broad arc. From north to south in the main part of the district, the axial trace of the arc strikes northeast to south-southwest (fig. 18). The Anaconda faults are most evident in the south-central part of the district, and overall they are recognized where the Steward faults have their most northeasterly strike. In contrast, Blue system faults occur along all reaches of the Steward faults irrespective of strike, and, to the east of the axis of the arc, the northeast fault-veins bend into the orientation of the Blue fault-veins.

4. There are distinctive zones of high-density horsetail normal faults between closely spaced east-northeast-to east-west–striking faults in the heart of the district. At the eastern tips of the master faults, the horsetail faults form a clockwise swarm of splays that fan to the right with mean splay angles to the master fault between 28°±7° and 35°±12° (n=40).

5. The faults and fault-veins parallel the directions of joints in the Late Cretaceous Butte Quartz
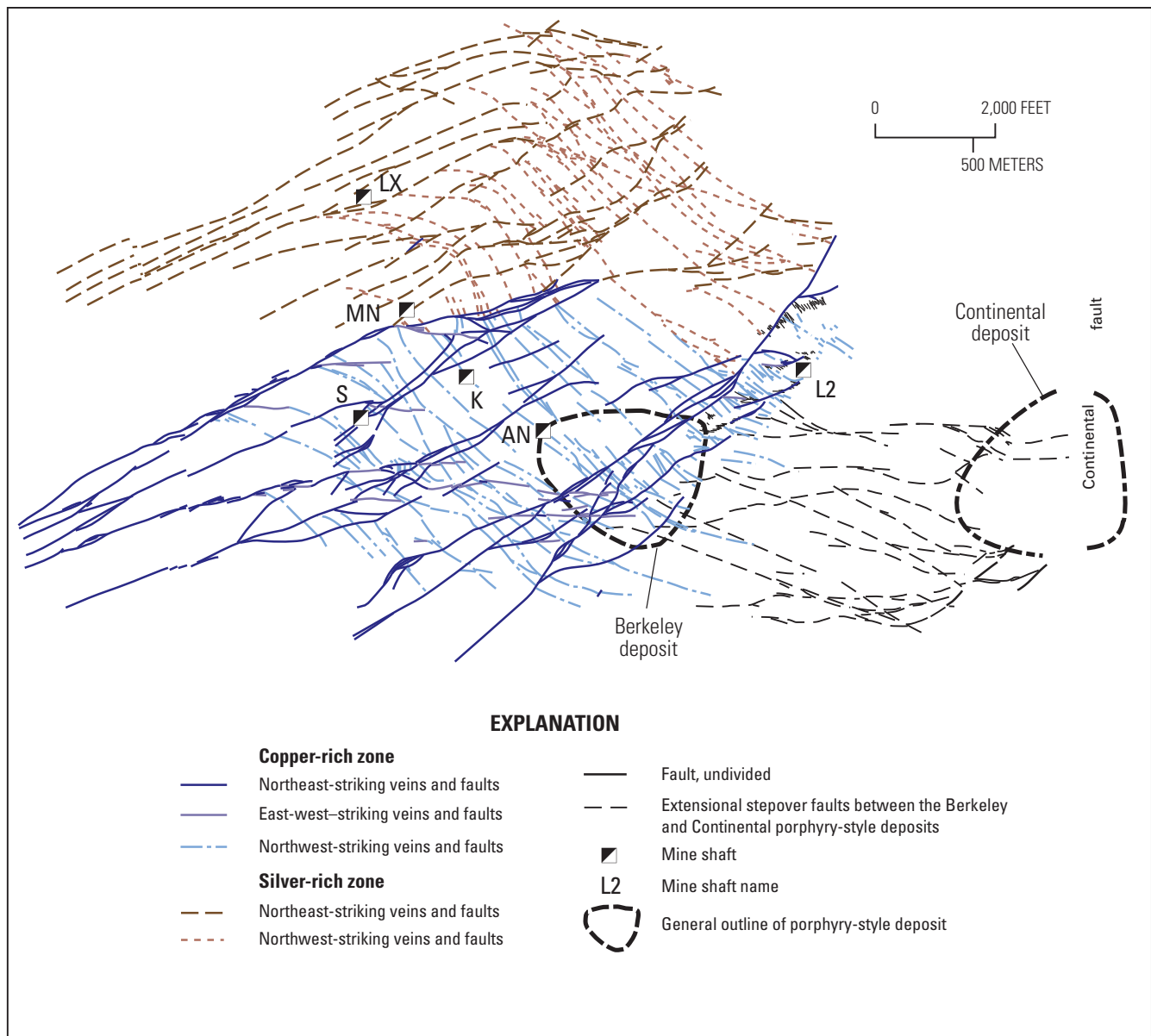
Figure 18.   Map of polymetallic quartz veins and faults in the Butte mining district. Those veins and associated faults that were predominantly mined for silver are color coded differently from those veins and faults predominantly mined for copper. Data for the dashed and solid lines are from veins on the 2,800-foot underground level, whereas data for the dashed lines in the southeast part of the map labeled as extensional stepover faults are from veins on the 4,600-foot underground level. (AN, Anaconda mine; K, Kelley mine; L2, Leonard No. 2 mine; LX, Lexington mine; MN, Mountain Consolidated mine; S, Steward mine; after Weed, 1912; Sales, 1914; Smedes, 1967, 1968; Meyer and others, 1968).

Monzonite. This correlation was noted originally by Weed (1912), who observed mineralized replacements of sheeted granite in the subsurface as well as some outcropping sheeted joints filled intermittently along strike with veins.

6. The spacing of mineralized fractures is, in general, irregular.

When taken as a whole, we suggest that these observations are consistent with an interpretation that faults in the district grew in a systematic and sequential manner wherein splay faults grew off the sides and especially at the tips of segmented, parallel northeast-striking right-lateral master faults. The splay faults formed uniform sets of structures because they were guided by the characteristic orientation of joints and fractures in the host Butte Quartz Monzonite. In this model, the northeast-striking faults are the master faults, and they appear to form a complex right-extensionally stepping array of northeast-striking master faults within which numerous splay faults were formed and propagated between their respective master structures. Our interpretation of the formation of the different fault sets (fig. 19) follows the models of Martel and Boger (1998) and Flodin and Aydin (2004).

Although much of the strain was accommodated through northeast-southwest extension parallel to the overall northeast trend of the vein-controlling master faults, curved traces of some splay faults between parallel master faults suggest that some measure of strain was accommodated through local clockwise rotation of the stress field. The predominance of extension parallel to the direction of strike-slip displacement is particularly evident in the zones of fans of extensional horsetail faults (fig. 19).

Discussion

Imprint of Proterozoic Deformation Fabrics on Boulder Batholith
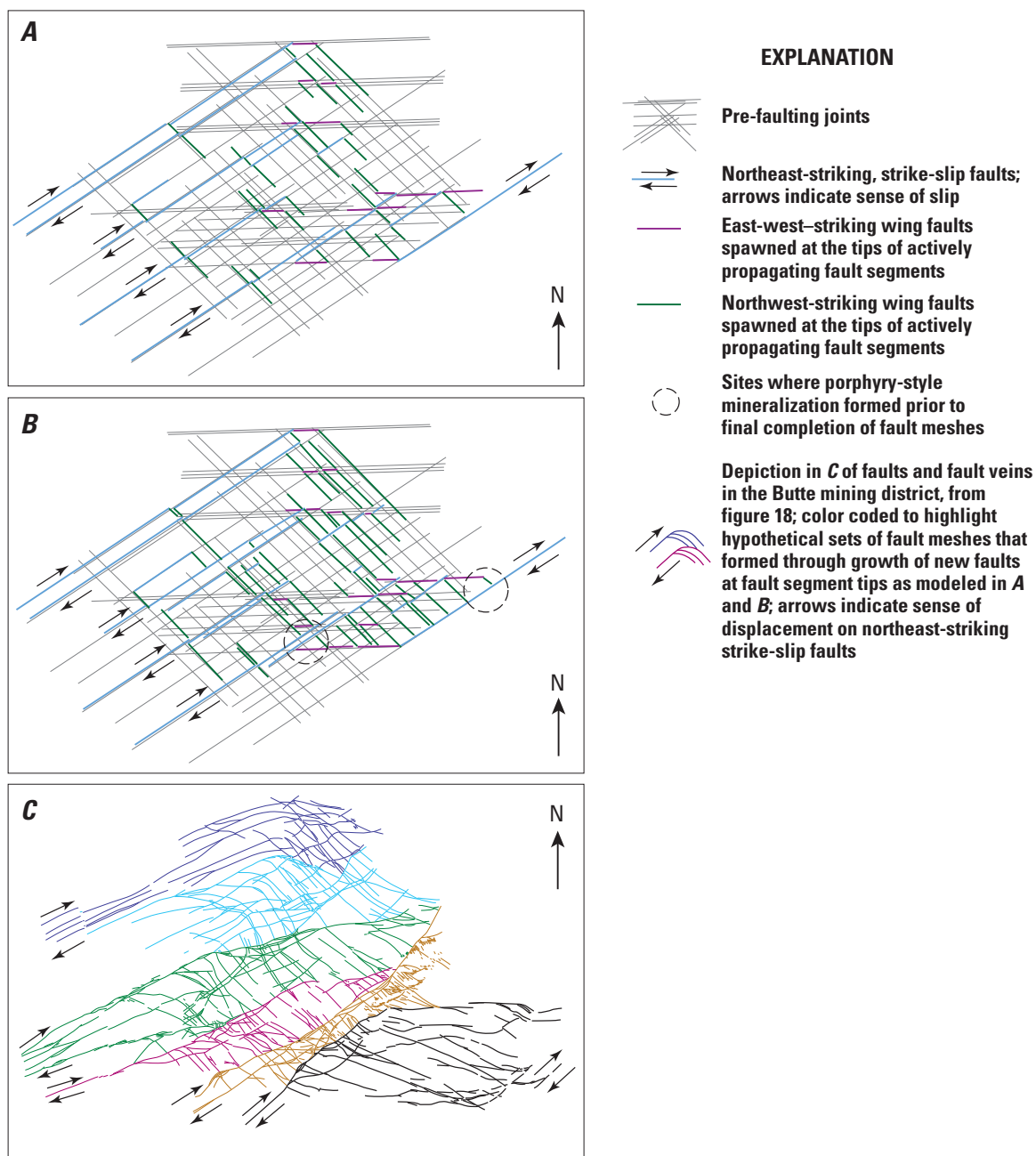
The Paleoproterozoic suturing and related events formed strong northeast- and east-west–trending deformation fabrics including faults, foliations, and lineations. Mesoproterozoic and Neoproterozoic deformations formed prominent northwest (fig. 4) and northeast as well as east-west fault fabrics (fig. 3). The reactivation of these various fault systems during Late Cretaceous to Early Tertiary tectonism has been widely recognized (for example, Harrison, 1972; Schmidt and Garihan, 1986. The influence of Precambrian faults on the emplacement of the Late Cretaceous Boulder batholith is particularly noticeable in the correspondence of the north and south boundaries of the batholith with the north and south fault boundaries of the Mesoproterozoic Helena embayment (fig. 4). As noted above, some lineaments mapped geophysically (fig. 9) within and to the southeast of the batholith are co-linear with mapped Proterozoic faults. Based on field data and the interpreted

geophysical lineament data, we infer that some early batholith-stage northwest-striking faults along the east and west sides of the batholith that localize dikes and some plutons (fig. 8) were reactivated Proterozoic structures. More problematic is the evidence from inside the Butte Quartz Monzonite. Here, structural trends as determined from fault and joint orientations, dike orientations, and geophysical lineaments generally strike northeast, but can they be linked to a Precambrian precursor? The corridor of Late Cretaceous dikes through the middle of the Butte Quartz Monzonite, the reactivation of this zone in the Paleocene at Butte, and again in the Eocene in the northern batholith (for example, Becraft and others, 1963), together with the U-Pb zircon dates (fig. 2), which are strongly divergent on either side of a northeast-trending line that passes through Butte, provide strong evidence that a Precambrian fault zone underlies the Butte Quartz Monzonite. Further, samarium and neodymium isotope ratios in Eocene volcanic rocks (Dudás and Ispolatov, 1997) near the city of Butte indicate a change in basement rock composition between areas northeast and southwest of the district, consistent with the underlying fault hypothesis of O'Neill (1998).

Shape and Controls on Emplacement of the Boulder Batholith

The thickness and controls on emplacement of the Boulder batholith and their relation to other Late Cretaceous tectonic elements have been the subject of debate for many years (for example, Lawson, 1914; Hamilton and Myers, 1967; Klepper and others, 1974; Schmidt and others, 1990; Kalakay and others, 2001). Klepper and others (1974) argued that the Boulder batholith is 10–20+ km thick, while Hamilton and Myers (1967) considered it to be a flat-bottomed sheet about 5 km thick. Schmidt and others (1990) modeled gravity data and calculated the thickness of the batholith to be about 15 km. They further proposed that the western half of the batholith is laccolithic, whereas the eastern half is a thick prism. Kalakay and others (2001) interpreted the batholith to have been emplaced as a composite tabular body at 1–10 km.

Our interpretation of the geological and geophysical data is consistent with some aspects of published models and in disagreement with others. In agreement with Hamilton and Myers (1967), our modeling shows the batholith to be a relatively thin slab, but our model disagrees with published interpretations that the batholith thickness exceeds 10 km (for example, Klepper and others, 1971a). Further, our modeling of the physical property data does not support a laccolithic geometry for the western half of the batholith, as proposed by Schmidt and others (1990). Based on geologic map and potential-field geophysical data, we believe the 80- to 76-Ma early-stage intrusions, after an initial stage of synthrust fault emplacement, were localized primarily by strike-slip and linked faults that accommodated strains behind the eastward-migrating thrust fault front, as may be seen in dike orientations illustrated in figure 10C.

EXPLANATION

Pre-faulting joints

Northeast-striking, strike-slip faults; arrows indicate sense of slip

East-west–striking wing faults spawned at the tips of actively propagating fault segments

Northwest-striking wing faults spawned at the tips of actively propagating fault segments

Sites where porphyry-style mineralization formed prior to final completion of fault meshes

Depiction in *C* of faults and fault veins in the Butte mining district, from figure 18; color coded to highlight hypothetical sets of fault meshes that formed through growth of new faults at fault segment tips as modeled in *A* and *B*; arrows indicate sense of displacement on northeast-striking strike-slip faults

The potential-field data indicate the later-stage Butte Quartz Monzonite is a generally symmetric body with inward-dipping sidewalls, a generally flat top, and a generally flat bottom. Where the side-margin contacts are exposed, field data are strongly suggestive that the northeast-elongate pluton was fault bounded. The strike of the western and eastern margins of the Butte Quartz Monzonite indicates a significant change in the dominant fault orientation from the more homogeneous northwest-southeast and northeast-southwest orientations during early-stage plutonism. Because all phases of the batholith were emplaced concurrent with thrust faulting, the major change in strain accommodation that occurred at approximately 76 Ma requires explanation. The structural model that best explains all of the available data and geometric relations is a pull-apart model similar to that proposed by Schmidt and others (1990).

Our modeling results and interpretation differ significantly from the interpretation of Schmidt and others (1990):

1. The potential-field geophysical data show that the Butte Quartz Monzonite is ringed (fig. 13A) by mafic, more magnetic early-stage intrusions.

2. In addition, the potential-field data preclude the west half of the Butte Quartz Monzonite from being laccolithic, as discussed above. Owing to the opposing displacement on east-west faults at the north and south sides of the Helena embayment as the thrust front continued to migrate east and the predominance of northeast-directed shear coupled with east-west extension within the Butte Quartz Monzonite, the Butte Quartz Monzonite is best modeled as having been localized within a pull-apart structure.

3. 3D geophysical modeling (fig. 16) indicates that the Butte Quartz Monzonite magma was likely intruded through two feeder zones, one in the north and the other in the south. This, taken together with the possible ringing of the north and south lobes by more magnetic early-stage intrusions is suggestive of a binodal pull-apart structure. This structure explains the differences between the north and south Butte Quartz Monzonite, such as the presence of abundant Butte Quartz Monzonite-related quartz-sulfide veins in the northern node but few in the south.

The mechanism by which the pull-apart opened is subject to constraints set by field observations, seismic profiles, and modeling of the potential-field geophysical data. The geometric relations that must be accounted for include the (1) the geometry of the batholith, including the east dip of its west edge and west dip of its east edge (see Vejmelek and Smithson, 1995); (2) bilateral symmetry of the Butte Quartz Monzonite across the zone of northeast-striking dikes, despite the coeval asymmetric advance of the thrust front farther east (fig. 6); (3) its <10-km thickness; and (4) the flattening strains in the east margin of the Butte Quartz Monzonite, along with a strong compression of the metamorphic rock or early-stage pluton footwall of the contact. We suggest that the most likely mechanism is a deep-seated, northeast-striking basement shear zone that extends diagonally beneath and across the long axis of the Butte Quartz Monzonite, likely a reactivation of a large Paleoproterozoic suture, the Great Falls tectonic zone, as hypothesized by O'Neill (1998). The possibility of such a zone was discussed previously, but Tertiary magmatism provides additional corroborative evidence. Northeast-striking Eocene

Figure 19. (facing page) Structural model of the origin of the faults and fractures that localized veins in the Butte mining district. In *A* and *B*, pre-fault joint trends are shown in light gray; faults are color coded according to whether the predominant strike is northeast (blue), east-west (magenta), or northwest (green). *A*, The initial stage of faulting consists of along-strike segmented, parallel north-northeast–striking to northeast-striking right-lateral strike-slip faults developed parallel to northeast-striking joints. At along-strike segment boundaries, small splay or wing faults with trends of east-west and northwest may develop on one or both sides of the master faults at segment tips. Parallel splay faults that propagate away from a master fault on opposite sides of the master do not necessarily form a singular line and thus may be interpreted as having been a singular fault that was offset by the master. As the northeast faults continue to propagate along strike, new splay faults may develop and preexisting splays may lengthen primarily in the direction of a northeast-striking master fault and, in turn, spawn new splay faults at their propagating tips as the system of faults grows in complexity. *B*, With continued shear stress on the master northeast-striking faults, the splay faults progressively propagate away from the master faults on one or both sides of the individual masters and begin to form linked mesh-form arrays of faults. New faults in the orientation of the master fault may develop at tips of wing faults between regional masters and also begin to propagate, thereby resulting in the formation of subnetworks within the larger-scale networks of faults. At Butte, northwest-striking faults accommodate the most extension within the shear system and thus are the most continuous and abundant extensional splay faults. Such arrays of northwest faults may grow sufficiently to intersect another master fault and complete a set of "horsetailing" faults. *C*, The complex networks of linked faults continue to develop until the northwestern-most northeast master fault is kinematically linked to the southeastern-most master fault. The fault patterns at Butte shown here suggest that the system of linked faults consists of at least six major groups, interpreted and color coded individually for illustrative purposes. It is interpreted that the hypothesized fault network groups acted to compartmentalize hydrothermal fluid flow during vein formation, leading to the general segregation of silver-rich and copper-rich veins as shown in figure 18.

dikes in the northern node of the Butte Quartz Monzonite are coincident with the Cretaceous dike trend (fig. 7) and form a 3-km-wide, 50-km-long corridor. In addition, there are also northeast-striking Tertiary faults and Oligocene dikes and veins along the same corridor. These relations require the batholith to be attached to the basement and not displaced east on a décollement; further, they support the presence of a high-angle zone of shear beneath the batholith. The inferred feeder zones for the Butte magma also fall along this linear zone.

Based on the east and west faulted margins of the Butte Quartz Monzonite and its overall bilateral symmetry across a northeast-trending line, we suggest that the pull-apart boundary faults likely root in the inferred northeast-striking fault zone beneath the Butte Quartz Monzonite. An implication of the bilateral symmetry and "rooting" interpretation is that the pull-apart grew from the bottom up. East and west spreading of the pull-apart could only happen in response to lateral displacement on the underlying northeast-striking basement shear zone. This shear was, in turn, a response to different rates of displacement on the east-west–striking faults bounding the Helena embayment as the thrust front moved asymmetrically east in response to east-west compression. This model differs from other interpretations that suggest a pull-apart driven by basal thrust detachment (for example, Schmidt and others, 1990; O'Neill and others, 2004). One or more pre-batholith décollements may have served as the base of the pull-apart, but they did not drive the structural systematics. A further difference is that our pull-apart driving mechanism does not require the eastward displacement of the batholith. Although geophysical data imply a somewhat broader zone of early-stage plutons to the east of the Butte Quartz Monzonite than to the west (for example, fig. 13*A*), the pull-apart very nearly bifurcated the early-stage batholith and the older plutons that now form a ring around the remarkably symmetric Butte Quartz Monzonite. Though Schmidt and others (1990) hypothesize that the northeast-striking fault zone served as a backstop to the pull-apart as the east margin moved east along the trailing edge of a thrust, that hypothesis is not supported by either the seismic data (Vejmelek and Smithson, 1995) or the potential-field data. Instead, the geophysical evidence suggests that the early-stage plutons increase in volume with depth and are rooted at least as deeply as the Butte Quartz Monzonite. We suggest that it is because of the pinning of the thrusts by pluton emplacement that strike-slip faults became the dominant mechanism for accommodating compression during early-stage plutonism and provided space for the intrusions.

Depth of Emplacement of Batholith

Houston (2002) argues on the basis of hornblende geobarometry in the Butte mining district that the Butte Quartz Monzonite was emplaced 7–9 km below its present level of exposure. However, it is highly likely that the top of the plutonic rocks was in the range of a 2- to 4-km depth because (1) vein textures in the Butte district more nearly reflect

epithermal and not mesothermal conditions, (2) plutons of all ages in the batholith intrude their own volcanic pile, (3) the roofs of the plutons are generally flat, (4) open-space filling quartz-carbonate-sulfide veins presumed related to the batholithic plutons are found near the roof-country rock contact of many stocks, and (5) some Elkhorn Volcanics eruptions, into which the Butte Quartz Monzonite intruded, formed calderas. The Butte Quartz Monzonite to the north and east of the city of Butte and the Rader Creek Granodiorite pluton to the southeast intrude the Elkhorn Mountains Volcanics.

Butte Mining District

Despite the greater intensity of faulting in the Butte mining district relative to elsewhere in the batholith, the orientations of the fault-veins are similar to the predominant fracture trends observed throughout the batholith (for example, fig. 10). This similarity suggests that joints representative of released stored regional strains in the Butte Quartz Monzonite had some control on development of the mineralized Butte fracture networks.

Our suggested coupled strike-slip–splay fault model for the formation of the different fault-vein sets in the Butte district has two important implications:

1. Because extension is northeast-southwest between northeast-striking strike-slip faults, fluid flow would have been effectively compartmentalized into generally northeast-trending panels bounded by parallel northeast-striking faults. This possibility is consistent with the paucity of ore along the master strike-slip faults because there is little extension *per se* within these faults.

2. Owing to the relatively low permeability of the northeast striking panel-bounding faults, hydrothermal fluid flow would have been predominantly vertical within a panel. The hydrogeology thus implies that the two types of polymetallic-vein mineralization (silver-zinc-lead, Ag-Zn-Pb, and copper-arsenic-zinc, Cu-As-Zn) did not form from the lateral flow of a single fluid with evolving composition. Two discrete fluids best explain the spatial separation and compositional differences.

Conclusions

The localization of the Boulder batholith plutons, dikes, veins, and fractures in the Great Falls tectonic zone, southwestern Montana, was influenced by a long history of intermittent deformation events involving the basement, some as old as 1,800 Ma. Intrusive and related volcanic activity began synchronously with superjacent thrust faulting, the fronts of which were guided by Proterozoic deformation zones. Shortly thereafter, the localization of plutons, dikes, and veins west of

the active thrust front was controlled by strike-slip and related faults that likely represent reactivated Proterozoic faults. Modeling of potential-field geophysical data using 2D and 3D methods is consistent with an interpretation that the late stage of the batholith was emplaced in a binodal pull-apart structure probably related to the reactivation of an underlying Paleoproterozoic suture zone-related fault. Asymmetric advance of the thrust front likely reactivated the suture-related fault owing to different rates of displacement on the east-west–trending north and south boundaries of the Helena salient wherein the thrust faults were active.

The principal Proterozoic deformation fabrics are recognizable in the orientations of fault-veins in the Paleocene Butte mining district. During the early Tertiary, northeast-striking joints in the Butte Quartz Monzonite above the basement suture-related fault were activated through shear resulting in right-lateral faulting across the district. At segment boundaries, that is where the progress of strike-slip displacement is interrupted, splay faults were formed along east-west and northeast trends, and the right-extensional stepping of the master northeast-striking faults resulted in a complex but systematic array of faults within which the Butte hydrothermal activity was localized.

Acknowledgments

References

Becraft, G.E., Pinckney, D.M., and Rosenblum, S., 1963, Geology and mineral deposits of the Jefferson City quadrangle, Jefferson and Lewis and Clark Counties, Montana: U.S. Geological Survey Professional Paper 428, 101 p.

Billingsley, P.R., and Locke, A., 1941, Structure of ore districts in the continental framework: Transactions, American Institute of Mining Engineers, v. 144, p. 9–59.

Blakeley, R.J., and Simpson, R.W., 1986, Locating edges of source bodies from magnetic and gravity anomalies: Geophysics, v. 51, p. 1394–1396.

Cole, M.M., 1983, Nature, age, and genesis of quartz-sulfide-precious metal vein systems in the Virginia City mining district, Madison County, Montana: Bozeman, Mont., Montana State University, M.S. thesis, 63 p.

Cordell, L., and Henderson, R.G., 1968, Iterative three-dimensional solution of gravity anomaly data using a digital computer: Geophysics, v. 33, p. 596–601.

Cordell, L., Keller, G.R., and Hildenbrand, T.G., 1982, Bouguer gravity map of the Rio Grande rift, Colorado, New Mexico, and Texas: U.S. Geological Survey Geophysical Investigations Map GP-949, scale 1:1,000,000.

Dudás, F.O., and Ispolatov, V.O., 1997, Nd, Sr and Pb isotopic composition of the Lowland Creek Volcanics, west-central Montana [abs.], *presented at* Seventh Annual V.M. Goldschmidt Conference, Tucson, Arizona: Lunar and Planetary Institute Contribution, v. 921, p. 62.

Eisele, J., and Isachsen, C.E., 2001, Crustal growth in southern Arizona—U-Pb geochronologic and Sm-Nd isotopic evidence for addition of the Paleoproterozoic Cochise block to the Mazatzal Province: American Journal of Science, v. 301, p. 773–797.

Emsbo, P., Groves, D.I., Hofstra, A.H., and Bierlein, F.P., 2006, The giant Carlin gold province—A protracted interplay of orogenic, basinal, and hydrothermal processes above a lithospheric boundary: Mineralium Deposita, v. 41, p. 517–525.

Flodin, E.A., and Aydin, A., 2004, Evolution of a strike-slip fault network, Valley of Fire State Park, southern Nevada: Geological Society of America Bulletin, v. 116, p. 42–59.

Foster, D.A., Mueller, P.A., Mogk, D.W., Wooden, J.L., and Vogl, J.J., 2006, Proterozoic evolution of the western margin of the Wyoming craton—Implications for the tectonic and magmatic evolution of the northern Rocky Mountains: Canadian Journal of Earth Science, v. 43, p. 1601–1619.

Grauch, V.J.S., and Cordell, L., 1987, Limitations of determining density and magnetic boundaries from the horizontal gradient and pseudogravity data: Geophysics, v. 52, p. 118–121.

Grauch, V.J.S., Rodriguez, B.D., and Wooden, J.L., 2003, Geophysical and isotopic constraints on crustal structure related to mineral trends in north-central Nevada and implications for tectonic history: Economic Geology, v. 98, p. 269–286.

Hamilton, W., and Myers, W.B., 1967, The nature of batholiths: U.S. Geological Survey Professional Paper 554-C, 29 p.

Harlan, S.S., Geissman, J.W., Lageson, D.R., and Snee, L.W., 1988, Paleomagnetic and isotopic dating of thrust-belt deformation along the eastern edge of the Helena salient, northern Crazy Mountains Basin, Montana: Geological Society of America Bulletin, v. 100, p. 492–499.

Harlan, S.S., Geissman, J.W., Snee, L.W., and Reynolds, R.L., 1996, Late Cretaceous remagnetization of Proterozoic mafic dikes, southern Highland Mountains, southwestern Montana—A paleomagnetic and ^{40}Ar/^{39}Ar study: Geological Society of America Bulletin, v. 108, p. 653–668.

Harrison, J.E., 1972, Precambrian Belt basin of northwestern United States—Its geometry, sedimentation, and copper occurrences: Geological Society of America Bulletin, v. 83, p. 1215–1240.

Hobbs, S.W., Griggs, A.B., Wallace, R.E., and Campbell, A.B., 1965, Geology of the Coeur d'Alene district, Shoshone County, Idaho: U.S. Geological Survey Professional Paper 478, 139 p.

Houston, R.A., 2002, Geology and structural history of the Butte district, Montana: Corvallis, Oreg., Oregon State University, M.S. thesis, 45 p.

Kalakay, T.J., Barbara, E.J., and Lageson, D.R., 2001, Fault-controlled pluton emplacement in the Sevier fold-and-thrust belt of southwest Montana: Journal of Structural Geology, v. 23, p. 1151–1165.

Karlstrom, K.E., and Humphreys, E.D., 1998, Persistent influence of Proterozoic accretionary boundaries in the tectonic evolution of southwestern North America—Interaction of cratonic grain and mantle modifications: Rocky Mountain Geology, v. 33, p. 161–179.

Klepper, M.R., Robinson, G.D., and Smedes, H.W., 1971a, On the nature of the Boulder batholith of Montana: Geological Society of America, v. 82, p. 1563–1580.

Klepper, M.R., Robinson, G.D., and Smedes, H.W., 1974, Nature of the Boulder batholith of Montana—Discussion: Geological Society of America Bulletin, v. 85, p. 1953–1960.

Klepper, M.R., Ruppel, E.T., Freeman, V.L., and Weeks, R.A., 1971b, Geology and mineral deposits, east flank of the Elkhorn Mountains, Broadwater County, Montana: U.S. Geological Survey Professional Paper 665, 66 p.

Klepper, M.R., Weeks, R.A., and Ruppel, E.T., 1957, Geology of the southern Elkhorn Mountains, Montana: U.S. Geological Survey Professional Paper 292, 82 p.

Knopf, A., 1963, Geology of the northern part of the Boulder batholith and adjacent area, Montana: U.S. Geological Survey Miscellaneous Geologic Investigations Map I-381, scale 1:48,000.

Lawson, A.C., 1914, Is the Boulder 'batholith' a laccolith?: University of California Publications in Geology, v. 8, p. 1–15.

Lund, K., Aleinikoff, J.N., Kunk, M.J., Unruh, D.M., Zeihen, G.D., Hodges, W.C., du Bray, E.A., and O'Neill, J.M., 2002, SHRIMP U-Pb and ^{40}Ar/^{39}Ar age constraints for timing of mineralization in the Boulder batholith, Montana: Economic Geology, v. 97, p. 241–267.

Martel, S.J., and Boger, W.A., 1998, Geometry and mechanics of secondary fracturing around small three-dimensional faults in granitic rock: Journal of Geophysical Research, v. 103, p. 21299–21314.

McCafferty, A.E., Bankey, V., and Brenner, K.C., 1998, Merged aeromagnetic and gravity data for Montana—A web site for distribution of gridded data and plot files: U.S. Geological Survey Open-File Report 98-0333, 20 p.

McCaffrey, K.J.W., and Petford, N., 1997, Are granitic intrusions scale invariant?: Journal of the Geological Society of London, v. 154, p. 1–4.

Mehnert, H.H., and Schmidt, R.G., 1971, Dating the Eldorado thrust: U.S. Geological Survey Professional Paper 750-A, 37 p.

Meyer, C., Shea, E.P., and Goddard, C.C., 1968, Ore deposits at Butte, Montana, *in* Ridge, J.D., ed., Ore deposits of the United States—The Graton-Sales volume (v. 2): New York, American Institute of Mining, Metallurgical, and Petroleum Engineers, p. 1373–1416.

Miller, R.N., 1973, Production history of the Butte district and geological function, past and present, *in* Miller, R.N., ed., Guidebook for the Butte field meeting of Society of Economic Geologists: Montana Bureau of Mines and Geology, Butte, p. F1–F10.

Murphy, J.G., Foster, D.A., Kalakay, T.J., John, B.E., and Hamilton, M., 2002, U-Pb zircon geochronology of the eastern Pioneer igneous complex, SW Montana—Magmatism in the foreland of the Cordilleran fold and thrust belt: Northwest Geology, v. 31, p. 1–11.

O'Neill, J.M., 1998, The Great Falls tectonic zone, Montana-Idaho—An Early Proterozoic collisional orogen beneath and south of the Belt basin, *in* Berg, R.B., ed., Belt Symposium III: Montana Bureau of Mines and Geology Special Publication 112, p. 227–234.

O'Neill, J.M., and Lopez, D.A., 1985, Character and regional significance of Great Falls tectonic zone, east-central Idaho and west-central Montana: American Association of Petroleum Geologists Bulletin, v. 69, p. 437–447.

O'Neill, J.M., Lund, K., Van Gosen, B.S., Desborough, G.A., Sole, T.C., and DeWitt, E.H., 2004, Geologic framework, chap D1 *of* Nimick, D.A., Church, S.E., and Finger, S.E., eds., Integrated investigations of environmental effects of historical mining in the Basin and Boulder mining districts, Boulder River watershed, Jefferson County, Montana: U.S. Geological Survey Professional Paper 1652, p. 53–88.

Prostka, H.J., 1966, Igneous geology of the Dry Mountain quadrangle, Jefferson County, Montana: U.S. Geological Survey Bulletin 1221-F, 21 p.

Reynolds, M.W., 1979, Character and extent of basin-range faulting, western Montana and east-central Idaho, *in* Newman, G.W., and Goode, H.D., eds., Basin and Range Symposium and Great Basin Field Conference, Las Vegas, Nev., 1979, Proceedings: Denver, Colo., Rocky Mountain Association of Geologists, p. 185–193.

Ruppel, E.T., 1963, Geology of the Basin quadrangle, Jefferson, Lewis and Clark, and Powell Counties, Montana: U.S. Geological Survey Bulletin 1151, 121 p.

Sales, R.H., 1914, Ore deposits at Butte, Montana: Transactions, American Institute of Mining Engineers, v. 46, p. 3–106.

Schmidt, C.J., and Garihan, J.M., 1986, Role of recurrent movement of northwest-trending basement faults in the tectonic evolution of southwestern Montana, *in* Aldrich, M.J., Jr., and Laughlin, A.W., eds., Proceedings of the Sixth International Conference on Basement Tectonics, Santa Fe, N. Mex., 16–20 September 1985: Salt Lake City, Utah, International Basement Tectonics Association, p. 1–15.

Schmidt, C.J., and O'Neill, J.M., 1982, Structural evolution of the southwest Montana transverse zone, *in* Powers, R.B., ed., Geologic studies of the Cordilleran thrust belt (v. 1): Denver, Colo., Rocky Mountain Association of Geologists, p. 193–218.

Schmidt, C.J., Smedes, H.W., and O'Neill, J.M., 1990, Syncompressional emplacement of the Boulder and Tobacco Root batholiths (Montana-USA) by pull-apart along old fault zones: Geological Journal, v. 25, p. 305–318.

Simpson, R.W., Jachens, R.C., Blakely, R.J., and Saltus, R.W., 1986, A new isostatic residual gravity of the conterminous United States, with a discussion of the significance of the isostatic residual anomalies: Journal of Geophysical Research, v. 91, p. 8348–8372.

Smedes, H.W., 1966, Geology and igneous petrology of the northern Elkhorn Mountains, Jefferson and Broadwater counties, Montana: U.S. Geological Survey Professional Paper 510, 116 p.

Smedes, H.W., 1967, Preliminary geologic map of the northeast quarter of the Butte South quadrangle, Montana, sheet 4 *of* Preliminary geologic map of the Butte South quadrangle, Montana: U.S. Geological Survey Open-File Report 67-203, scale 1:24,000.

Smedes, H.W., 1968, Preliminary geologic map of part of the Butte North quadrangle, Silver Bow, Deer Lodge, and Jefferson Counties, Montana: U.S. Geological Survey Open-File Report 68-254, scale 1:36,000.

Snee, L.W., Miggins, D., Geissman, J., Reed, M., Dilles, J., and Zhang, L., 1999, Thermal history of the Butte porphyry system, Montana: Geological Society of America Abstracts with Program, v. 31, p. 380.

Tilling, R.I., 1968, Zonal distribution of variations in structural state of alkali feldspar within the Rader Creek Granodiorite pluton, Boulder batholith, Montana: Journal of Petrology, v. 9, p. 331–357.

Tysdal, R.G., 1998, Revisions of Cretaceous Slim Sam Formation, western Montana: U.S. Geological Survey Professional Paper 1601-B, 8 p.

Vejmelek, L., and Smithson, S.B., 1995, Seismic reflection profiling in the Boulder batholith, Montana: Geology, v. 23, p. 811–814.

Webring, M., 1981, MINC—A gridding program based on minimum curvature: U.S. Geological Survey Open-File Report 81-1224, 43 p.

Webring, M., 1985, SAKI—Fortran program for generalized linear inversion of gravity and magnetic profiles: U.S. Geological Survey Open-File Report 85-122, 29 p.

Weed, W.H., 1912, Geology and ore deposits of the Butte district, Montana: U.S. Geological Survey Professional Paper 74, 262 p.

Wier, K.L., 1982, Maps showing geology and outcrops of part of the Virginia City and Alder quadrangles, Madison County, Montana: U.S. Geological Survey Miscellaneous Field Studies Map MF-1490, scale 1:12,000.

Winston, D., 1986, Middle Proterozoic tectonics of the Belt basin, western Montana and northern Idaho: Montana Bureau of Mines and Geology Special Publication 94, p. 245–257.